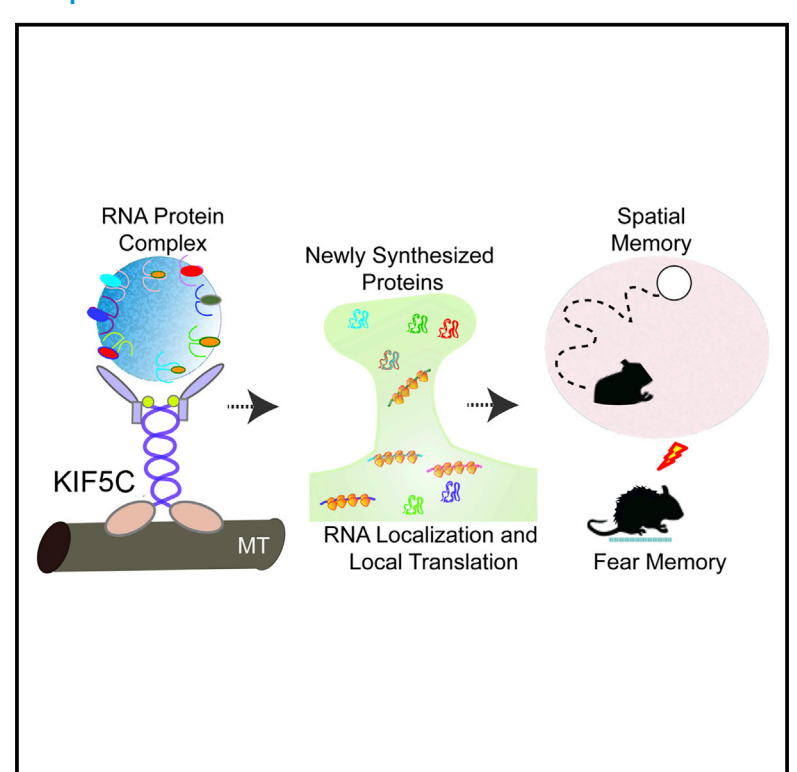
Molecular motor protein KIF5C mediates structural plasticity and long-term memory by constraining local translation

Graphical abstract



Authors

Supriya Swarnkar, Yosef Avchalumov, Isabel Espadas, ..., Damon Page, Kyle Miller,

Sathyanarayanan V. Puthanveettil

Correspondence

sputhanv@scripps.edu

In brief

Swarnkar et al. show that molecular motor KIF5C is a critical regulator of excitatory synaptic transmission, structural plasticity, and local translation. While knockdown of KIF5C impairs both contextual and spatial memory, its overexpression specifically enhances spatial memory.

Highlights

- KIF5C expression constrains excitatory synaptic transmission and structural plasticity
- KIF5C mediates the long-distance transport of substrates of local translation
- EIF3G modulates the effects of KIF5C on dendritic arborization and spine morphology
- Overexpression of KIF5C in CA1 neurons enhances spatial memory







Article

Molecular motor protein *KIF5C* mediates structural plasticity and long-term memory by constraining local translation

Supriya Swarnkar,¹ Yosef Avchalumov,^{1,4} Isabel Espadas,^{1,4} Eddie Grinman,¹ Xin-an Liu,^{1,5} Bindu L. Raveendra,¹ Aya Zucca,¹ Sonia Mediouni,² Abhishek Sadhu,¹ Susana Valente,² Damon Page,¹ Kyle Miller,³ and Sathyanarayanan V. Puthanveettil^{1,6,*}

SUMMARY

Synaptic structural plasticity, key to long-term memory storage, requires translation of localized RNAs delivered by long-distance transport from the neuronal cell body. Mechanisms and regulation of this system remain elusive. Here, we explore the roles of KIF5C and KIF3A, two members of kinesin superfamily of molecular motors (Kifs), and find that loss of function of either kinesin decreases dendritic arborization and spine density whereas gain of function of *KIF5C* enhances it. *KIF5C* function is a rate-determining component of local translation and is associated with ~650 RNAs, including *EIF3G*, a regulator of translation initiation, and plasticity-associated RNAs. Loss of function of *KIF5C* in dorsal hippocampal CA1 neurons constrains both spatial and contextual fear memory, whereas gain of function specifically enhances spatial memory and extinction of contextual fear. *KIF5C*-mediated long-distance transport of local translation substrates proves a key mechanism underlying structural plasticity and memory.

INTRODUCTION

Transcription activation and local translation leading to structural plasticity at the synapse are critical components of long-term memory (LTM) in sea slugs (Alberini et al., 1994; Martin et al., 1997; Miniaci et al., 2008), worms (Kwak et al., 2008; Sharifnia and Jin, 2015), flies (Davis, 2011; Pai et al., 2013; Wu et al., 2017), and mammals (Bekinschtein et al., 2008; Fioriti et al., 2015; Nakayama et al., 2017). In sensory and motor neurons of sea slug Aplysia, a homolog (ApKHC1) of a member of the Kinesin superfamily of proteins (Kifs) plays a key role in coordinating transcriptional and translational changes associated with LTM (Puthanveettil et al., 2008; Puthanveettil, 2013). Kifs are molecular motors moving from the minus end of microtubules to the plus end, mediating long-distance transport of organelles (Nangaku et al., 1994; Sekine et al., 1994), proteins (Kanai et al., 2004; Liu et al., 2014; Ohashi et al., 2002; Puthanveettil et al., 2008), and RNAs (Dictenberg et al., 2008; Lyons et al., 2009; Puthanveettil, 2013). Long-distance transport by specific Kifs could be modulated to regulate the availability of gene products at synapse—although the role of Kifs in coordinating communication between genes and synapses remains unclear.

Few studies show the role of Kifs in structural plasticity and LTM, either. Transgenic mice lacking KIF21B showed learning and memory deficits (Morikawa et al., 2018; Muhia et al., 2016), and studies reflect cumulative effects of loss of function in the entire animal or large brain areas from early development. Mice overexpressing KIF17 in the forebrain showed improved spatial memory (Wong et al., 2002), and Zhao et al. (2020) found that conditional KIF5B knockout results in hippocampal long-term potentiation (LTP) deficits for learning and memory. Whether expression of Kifs in specific neuronal populations constrains LTM, how the Kifs are regulated, and how they function are all lingering questions. Compositions of cargos transported by Kifs, critical for memory storage, remain equally elusive. We executed loss-offunction and gain-of-function experiments in vitro and in vivo to assess whether manipulation of kinesin restricted to CA1 neurons of the hippocampus impacts learning and memory.

We first assessed the role of long-distance transport in neuronal morphology. Loss of function of two Kifs (*KIF3A*, a Kinesin-2 family member, and *KIF5C*, a Kinesin-1 family member) expressed in the same hippocampal (HP) neuron (Liu et al., 2014) diminished excitatory synaptic transmission, dendritic arborization, synapse density, and morphology. We found that the expression of *KIF5C*



¹Department of Neuroscience, Scripps Florida, 130 Scripps Way, Jupiter, FL 33458, USA

²Department of Immunology and Microbiology, Scripps Florida, 130 Scripps Way, Jupiter, FL 33458, USA

³Department of Integrative Biology, Michigan State University, East Lansing, MI, USA

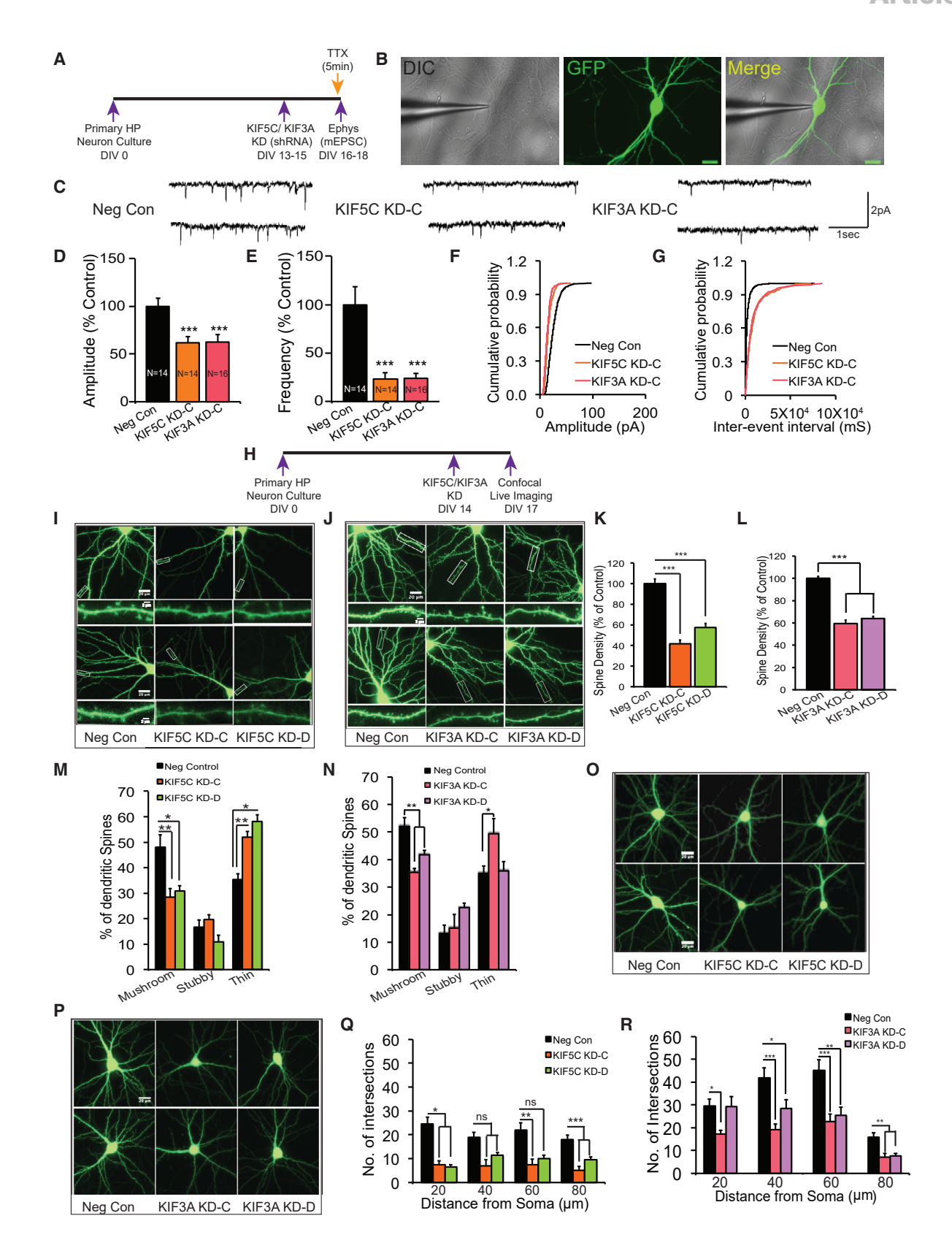
⁴These authors contributed equally

⁵Present address: The Brain Cognition and Brain Disease Institute, Shenzhen Institute of Advanced Technology, Chinese Academy of Sciences, Shenzhen 518055, China

⁶Lead contact

^{*}Correspondence: sputhanv@scripps.edu https://doi.org/10.1016/j.celrep.2021.109369





Article



constrains local translation, a key mechanism determining structural plasticity at the synapse. Furthermore, KIF5C expression in dorsal CA1 neurons of the mouse hippocampus constrains spatial memory and contextual fear memory. Together, these observations shed mechanistic insight into Kif-mediated regulation of local translation, structural plasticity, and LTM.

RESULTS

Expression of KIF5C and KIF3A necessary for excitatory synaptic transmission and maintenance of spines and dendritic arbors

Since structural plasticity underlies LTM, we asked whether KIF5C and KIF3A differentially impact spine density and dendritic arborization, as they are associated with distinct protein cargos. We reasoned that both Kifs could be critical for synapse function, but that specific knockdown (KD) of either would result in a distinct phenotype. Loss of function could also produce a similar phenotype because the distinct pathways regulated by each are critical components governing synapse function and architecture. Following RNAi-mediated KDs, we studied excitatory synaptic transmission, spine density, spine morphology, and dendritic arborization in mature HP neurons. In primary HP neuronal cultures, spines begin to form within 7-9 days in vitro (DIV) and mature from DIV 17 (Hayashi et al., 2011; Rui et al., 2013).

First, we measured the effect of KIF5C or KIF3A KD on miniature excitatory postsynaptic currents (mEPSCs). Because mEPSC amplitude is directly related to postsynaptic strength—whereas frequency is correlated with presynaptic release and inputs from a large number of synapses (Turrigiano et al., 1998) — we assumed that mEPSC measurements would distinguish pre- and postsynaptic effects of Kif KD, suggesting whether KD of different Kifs produces different effects on excitatory synaptic transmission. A scrambled nontargeting short hairpin RNA (shRNA) acted as control. Electrophysiology measurements showed significant reduction in amplitude and frequency of mEPSCs in Kif KD neurons (n = 14, p = 0.0009, one-way ANOVA followed by post hoc Tukey test; Figures 1A-1G; Table S1), suggesting the involvement of pre- and postsynaptic mechanisms. A multiplicative shift in mEPSC amplitude is a proven indicator of cell-wide changes in synaptic strength (O'Brien et al., 1998; Turrigiano et al., 1998). Our calculations of multiplicative shifts in KD neurons (KIF5C KD, 0.61; KIF3A KD, 0.62; relative to control) suggest that both KIF5C and KIF3A KD reduce synaptic strength across excitatory synapses, meaning expression of both KIF5C and KIF3A is critical for excitatory synaptic transmission contributed by both functional and morphological changes at synapse (Figures S1A-S1P).

We next examined spine density and morphology. Two different shRNAs (KD-C and KD-D) knocked down KIF5C and KIF3A expression in DIV 14 neurons. Spine morphology and dendritic branching at DIV 17 were analyzed by confocal live-cell imaging. Both KIF5C KD and KIF3A KD reduced total spine density in HP neurons (n = 9, ***p < 0.0001, one-way ANOVA followed by post hoc Tukey test; Figures 1H-1L; Table S1).

We then examined effect of KDs on synapse morphology, particularly mushroom spines-called "memory spines"-for their correlation with synaptic plasticity and memory (Mahmmoud et al., 2015). We found a significant decrease (~20%) in mushroom spines in KIF5C KD-C and KIF5C KD-D neurons compared to control. No significant changes were observed in stubby spine morphology with KIF5C KD compared to control, but there was a significant increase in thin spines (~15%) with KIF5C KD-C and KIF5C KD-D compared to control (Figure 1M; Table S1). KIF3A KD produced similar effects: $\sim 15\%$ reduction in mushroom spines in KIF3A KD-C and KIF3A KD-D neurons compared to control (Figure 1N), but no significant difference in stubby spines or thin spines compared to control (*p < 0.05, **p < 0.005, one-way ANOVA followed by post hoc Tukey test; Table S1).

Next, we examined Kif KD on dendritic arborization. Quantitative analysis of dendritic arbor by Sholl method (Raveendra et al., 2018) revealed significant differences in dendritic arborization following KIF5C or KIF3A KD (Figures 10 and 1P). We analyzed number of dendrites from 20 µm of soma and arborization changes up to 80 µm. Significant reduction in dendritic branching occurred in both KIF5C and KIF3A KD neurons (Figures 1Q and 1R; one-way ANOVA followed by post hoc Tukey test, *p < 0.05, **p < 0.005, ***p < 0.0005; Table S1). This suggests that both KIF5C and KIF3A play critical roles in excitatory synaptic transmission and neuronal architecture.

Gain of function of KIF5C but not KIF3A in HP neurons enhances mEPSCs

To assess whether long-distance transport mediated by Kifs is sufficient for synapse function and structural plasticity, we

Figure 1. KIF5C and KIF3A are necessary for excitatory synaptic communication, maintenance of spine morphology, and dendritic arbor-

(A) Experimental strategy to record mEPSCs in mouse primary HP neuronal cultures following KD of KIF5C and KIF3A using shRNAs.

(B) eGFP-labeled neurons in fluorescence and bright-field (BF) images with patch-clamp recording electrodes attached.

(C) Two traces of mEPSCs for negative control, or NC (scrambled shRNA), and shRNAs against KIF5C and KIF3A.

(D and E) Changes in amplitudes and frequencies of mEPSCs 72 h after KD of KIF5C and KIF3A. Number of neurons patched per group is labeled. Data (mean) from all KD groups compared to negative control.

(F and G) Changes in amplitude and frequency, respectively, of mEPSCs between NC and KIF5C or KIF3A shRNA (Kolmogorov-Smirnov test, p < 0.05).

(H) Experimental plan for KIF5C KD and confocal live imaging.

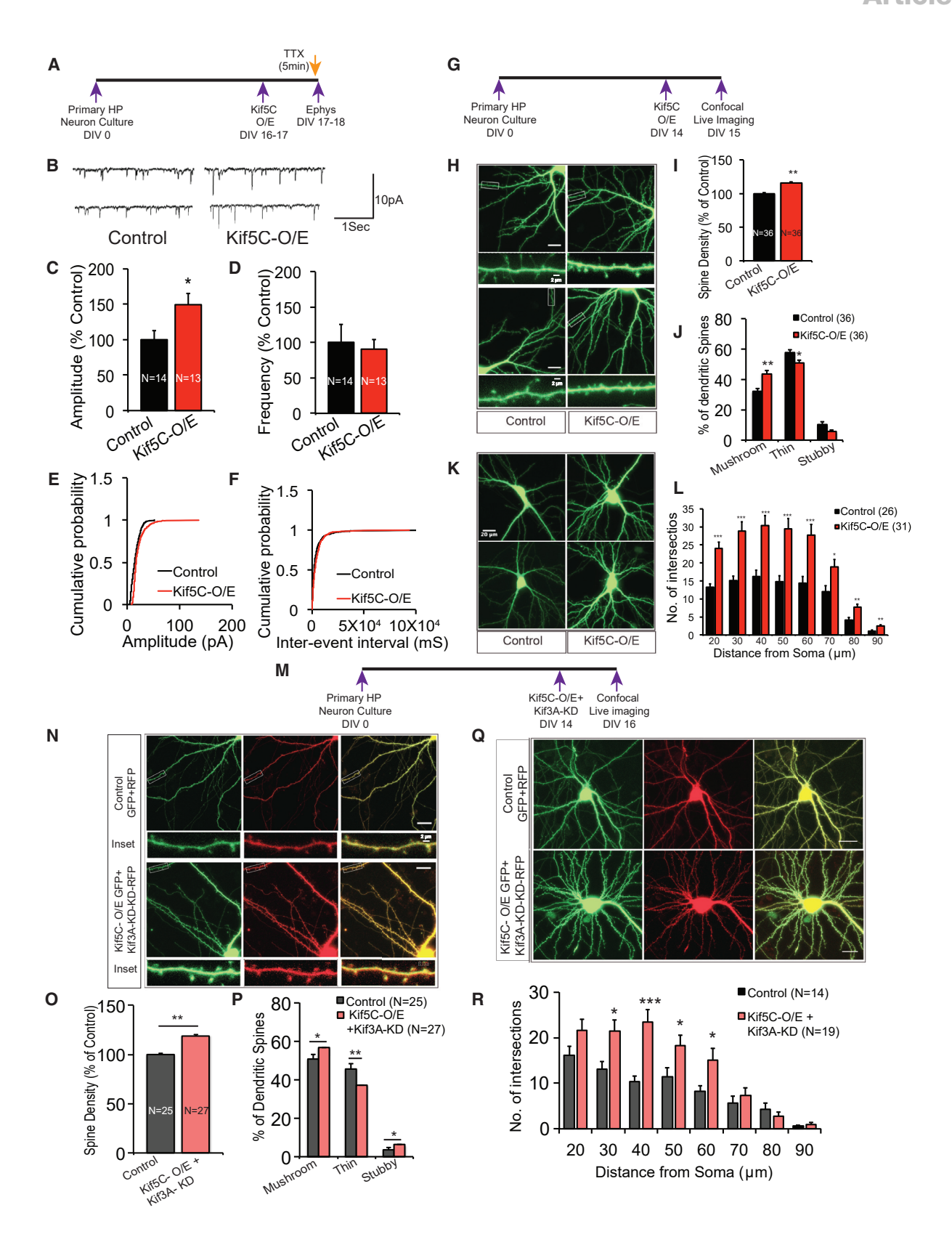
(I and J) Confocal projection images showing changes in spine, digitally enlarged image in inset.

(K-N) Quantitative analyses of image data shown in (I) and (J) executed by selecting dendrites with length of 100 µm. Bar graphs show change in spine density or morphology.

(O and P) Confocal projection images show soma in center to depict dendritic arbor.

(Q and R) Quantification of dendritic morphology changes in terms of number of intersections per 20-µm step size by Sholl analysis. Changes compared between KIF5C KD or KIF3A KD and NC. One-way ANOVA followed by Tukey's post hoc test. Error bars represent SEM. *p < 0.05, *p < 0.005, and ***p < 0.0005. Scale bar: 2 or 20 μm.





Article



performed gain-of-function analyses to study effects of overexpression (OE) of KIF5C and KIF3A in HP neurons by cloning fulllength (FL) cDNAs and expressing them as eGFP fusion proteins (C terminus) under control of CMV promoter in HP neurons. After confirming that KIF5C and KIF3A OE constructs are functional and results in enhanced transport of protein cargos in HP neurons (see STAR Methods), we asked whether OE of the Kifs changes synaptic transmission and executed whole-cell patchclamp recording to measure mEPSCs after 24 h of transfection in Kif OE primary HP neurons at DIV 16-17. Amplitude of mEPSCs significantly increased in KIF5C-overexpressing neurons compared to control eGFP neurons (p = 0.021; unpaired, two-tailed Student's t test). Change in frequency was comparable between KIF5C-overexpressing neurons and controls (p = 0.75; unpaired, two-tailed Student's t test; Figures 2A-2F; Table S1), suggesting specific effect on mEPSC components. Next, we recorded mEPSCs after overexpressing KIF3A in primary neurons and found no change in amplitude or frequency with KIF3A OE compared to control (p > 0.05; unpaired, two-tailed Student's t test; Figures S2A-S2F; Table S1). This indicates that KIF5C OE impacts a specific component of mEPSCs sufficient for enhancing excitatory synaptic transmission, whereas KIF3A OE is insufficient to produce synaptic enhancements in HP neurons. The multiplicative shift between OE and eGFP control neurons (KIF5C OE, 1.49; KIF3A OE, 0.94; compared to eGFP alone) suggests that, in contrast to KIF3A, KIF5C OE enhances strength of excitatory synapses.

Gain of function of KIF5C in HP neurons enhances dendritic arborization and synapse density

We next examined whether KIF5C OE change spine morphology and dendritic arborization. If enhancing dendritic localization of cargos by OE alone produces long-term change in morphology, we anticipated enhanced spine density, morphology, and dendritic arborization. We used DIV 14 cultures to overexpress KIF5C and analyzed spine morphology and dendritic branching at DIV 15. Neurons expressing eGFP alone served as controls. Consistent with our electrophysiological results, confocal livecell imaging showed KIF5C OE in HP neurons increasing total spine density compared to controls. We also observed significant increase in mushroom spines in KIF5C OE neurons compared to controls. Significant decrease in thin spines was observed in OE neurons, with no significant change in stubby spines (n = 36; p < 0.005 unpaired, two-tailed Student's t test; Figures 2G-2J; Table S1).

We then assessed KIF5C OE's effect on dendritic arborization. Sholl analysis showed KIF5C OE significantly increased dendritic branching, starting at 20 to 80 μm in HP neurons (Figures 2K–2L; Table S1) and suggesting that increased expression of KIF5C can produce new branching points in HP neurons.

We next asked whether KIF5C OE recruits KIF3A to enhance synapse density and dendritic arborization. Our analysis of spine density and dendritic arborization in neurons that overexpress KIF5C but deplete KIF3A suggested that enhancements in spine density, mushroom spines, and dendritic arborization (p < 0.01; unpaired, two-tailed Student's t test; Figures 2M-2R; Table S1) in KIF5C OE neurons are independent of KIF3A levels (see STAR Methods).

cAMP-PKA signaling regulates KIF5C expression and function

Modulation of synaptic transmission and architecture by KIF5C expression implied that KIF5C may play a key role in LTM, associated with remodeling synaptic connections. We determined whether learning-related signaling regulates KIF5C expression and therefore asked whether activating cAMP signaling could enhance KIF5C mRNA levels, as the cAMP-PKA signaling pathway is critical for learning and memory (Bacskai et al., 1993; Kandel 2012; Ma et al., 2009). We examined changes in mRNA expression of KIF5C after stimulating HP neurons with forskolin, an activator of adenylyl cyclase and cAMP signaling. We observed significantly increased relative gene expression of KIF5C (1.5 \pm 0.14; n = 3) 30 min after forskolin treatment. Upregulated gene expression is blocked by treatment with PKA inhibitor 14-22 amide (cell-permeable specific inhibitor of PKA), suggesting that KIF5C mRNAs are upregulated by forskolin in a PKA-dependent manner (1.15 \pm 0.11; n = 3; *p < 0.005, one-way ANOVA followed by post hoc Tukey test; Figures 3A and 3B; Table S1).

Figure 2. Overexpression (OE) of KIF5C enhances excitatory synaptic transmission, density of mushroom spines, and dendritic arborization (A) Experimental strategy to record mEPSCs in mouse primary HP neuronal cultures following OE of KIF5C and KIF3A using full-length cDNA expressing plasmids.

(B) Two traces of mEPSCs for control, KIF5C OE and KIF3A OE.

(C and D) Changes in amplitudes and frequencies of mEPSCs 24 h after KIF5C OE.

(E and F) Changes in amplitude and frequency of mEPSCs between control and KIF5C OE groups (Kolmogorov-Smirnov test, p < 0.05).

(G) Experimental plan for overexpressing KIF5C for confocal live imaging.

(H) Confocal projection images of KIF5C OE showing spine changes, digitally enlarged image in inset.

(I and J) Quantitative analyses of image data shown in (H) executed by selecting dendrites with length of 100 µm. Bar graphs show change in spine density or morphology

(K) Confocal projection images of KIF5C OE show soma in center to depict dendritic arbor.

(L) Quantification of dendritic morphology changes in terms of number of intersections per 10-μm step size by Sholl analysis.

(M) Experimental plan for KIF3A KD and KIF5C OE in same neuron for confocal live imaging.

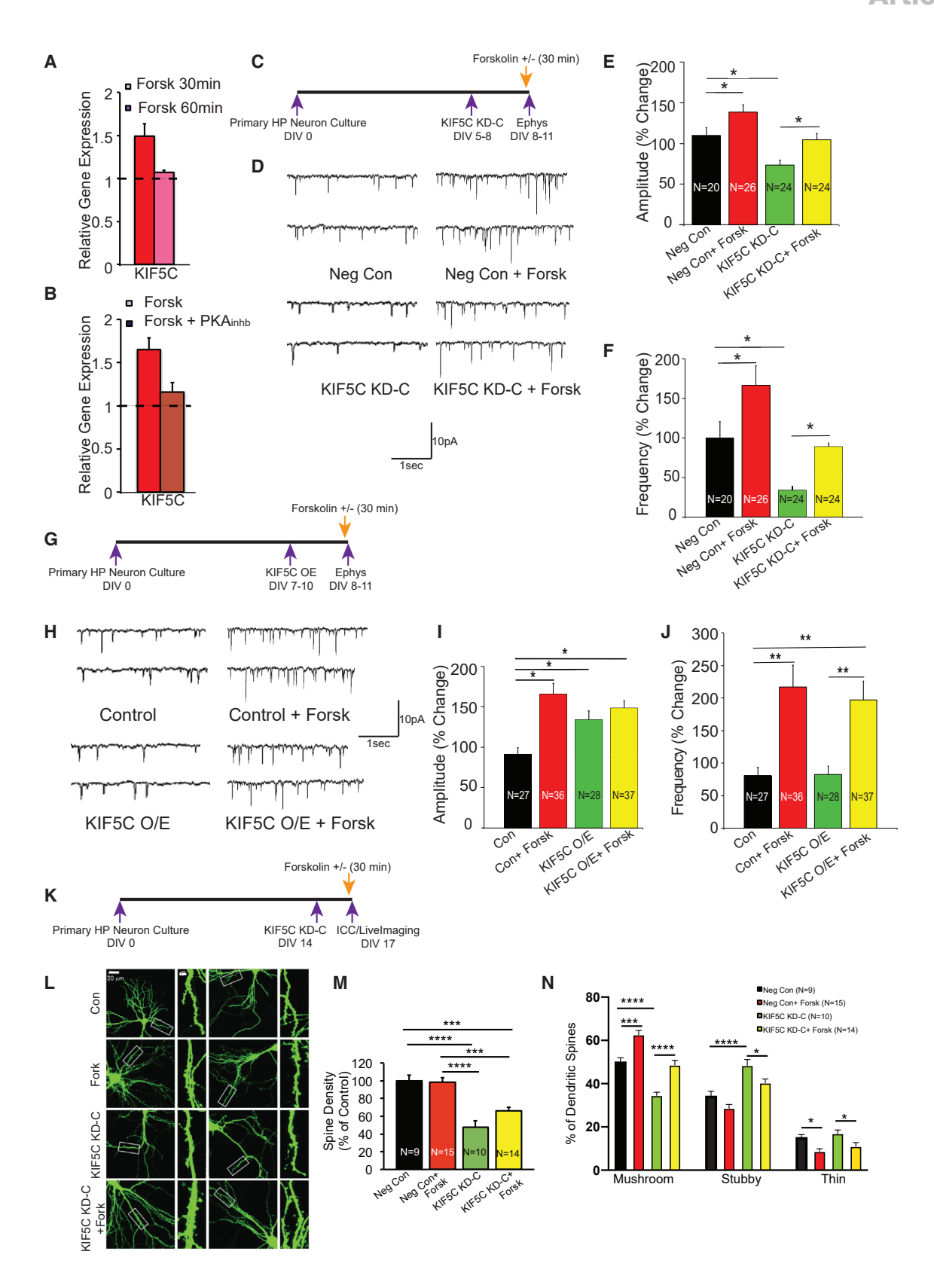
(N) Confocal projection images showing changes in spine, digitally enlarged image in inset.

(O and P) Quantitative analyses of image data shown in (N) achieved by selecting dendrites with length of 100 µm. Bar graphs show change in spine density or morphology.

(Q) Confocal projection images show soma in center to depict dendritic arbor.

(R) Quantification of dendritic morphology changes in terms of number of intersections per 10-µm step size by Sholl analysis. Changes compared between KIF5C OE and control, or changes compared between neurons with KIF5C OE and KIF3A KD to control eGFP- and RFP-expressing neurons. Unpaired, two-tailed Student's t test. Error bars represent SEM. *p < 0.05, *p < 0.005, and ***p < 0.0005. Scale bar: 2 or 20 μ m.





Article



To determine whether KIF5C expression impacts cAMPdependent changes in synaptic transmission and spine morphology, we measured forskolin-induced changes in mEPSCs in neurons with either KIF5C KD or OE. Consistent with prior data (Raveendra et al., 2018; Bie and Pan, 2005; Chen and Regehr, 1997), we found forskolin exposure increased mEPSC amplitudes and frequencies. Increase in amplitude for mEPSCs was significantly reduced in KIF5C KD neurons compared to nontargeting shRNA control. Frequency changes in mEPSCs in the forskolin + KIF5C KD group were significantly higher than those in the KIF5C KD group alone (p < 0.0001, oneway ANOVA followed by post hoc Holm-Sidak test; Figures 3C-3F; Figures S2G and S2H; Table S1). mEPSC frequencies and amplitudes in forskolin + KIF5C KD neurons did not reach levels of forskolin alone, indicating that KIF5C is essential for forskolininduced changes in synaptic transmission.

We observed no significant difference in forskolin-induced changes in mEPSC amplitude in KIF5C OE neurons compared to vehicle control. Change in frequency was comparable between control and KIF5C OE, whereas we observed a significant increase in frequency of forskolin-treated KIF5C OE neurons compared to KIF5C OE neurons alone (p < 0.0001, one-way ANOVA followed by post hoc Holm-Sidak test; Figures 3G-3J; Figures S2I and 2J; Table S1). Although KIF5C OE alone could increase mEPSC amplitudes, an additional increase in mEPSC amplitude was unobserved in the presence of forskolin, likely due to a ceiling effect on mEPSC amplitudes in KIF5C OE neurons. Consistent with prior data, spine morphology analysis indicated that KIF5C partly mediates mushroom spine morphology changes induced by cAMP signaling (*p < 0.01, *p < 0.001, and ***p < 0.0001, one-way ANOVA followed by post hoc Tukey test; Figures 3K-3N; Table S1; STAR Methods).

KIF5C regulates local translation

Through long-distance transport of RNAs, KIF5C may regulate availability of substrates for local translation. We therefore assessed whether forskolin-dependent changes in local translation require KIF5C. Having confirmed the quality of synaptoneurosome preparation (see STAR Methods), we studied effects of KIF5C KD on local translation by measuring peif2a/eif2a in synaptoneurosome proteins. After 72 hours of KIF5C KD, neuronal cultures were treated with forskolin or vehicle for 30 min. Synaptoneurosomes were isolated from control and KIF5C KD alone cells along with forskolin + KIF5C KD neurons. By quantifying changes in ratio of peif2a/eif2a, we found significant increase in ratio in KIF5C siRNA KD synaptoneurosomes (137.32 ± 12.92) compared to control (100 \pm 9.88), suggesting diminished translation in KIF5C KD synaptoneurosomes (n = 7, *p = 0.0486, one-way ANOVA; Figures 4A-4C; Figures S3A-S3F; Table S1). peif2a/eif2a ratios were comparable between KIF5C KD and forskolin + KIF5C KD synaptoneurosomes, suggesting KIF5C's role in modulating local translation.

We questioned whether an increase in KIF5C levels resulted in enhanced local translation. First, we carried out puromycin labeling (Ravi et al., 2018) of newly synthesized proteins (STAR Methods) and asked whether KIF5C OE in HP neurons changes puromycin-labeled proteins. We then studied whether KIF5C OE enhances local translation. Western blot (WB) analysis of synaptoneurosomes (Figures 4D-4F) showed KIF5C OE increased puromycin-labeled proteins, suggesting enhancement in local translation in KIF5C OE neurons (210.62 ± 29.6) compared to control (100 \pm 24.5; n = 3; *p < 0.01; unpaired, two-tailed Student's t test; Figure 4F; Figures S3G-S3I; Table S1). To confirm, we immunostained primary neurons. KIF5C OE resulted in increased staining of puromycin-labeled proteins in dendrites $(1,204.3 \pm 452.1, n = 8)$ when compared to eGFP control $(452.10 \pm 174.7, n = 7; **p < 0.001; unpaired, two-tailed Stu$ dent's t test; Figures 4G and 4H; Figures S3J-S3K; Table S1). This suggests that KIF5C is a key mediator of local translation in HP neurons.

KIF5C mediates long-distance transport of molecular substrates of local translation

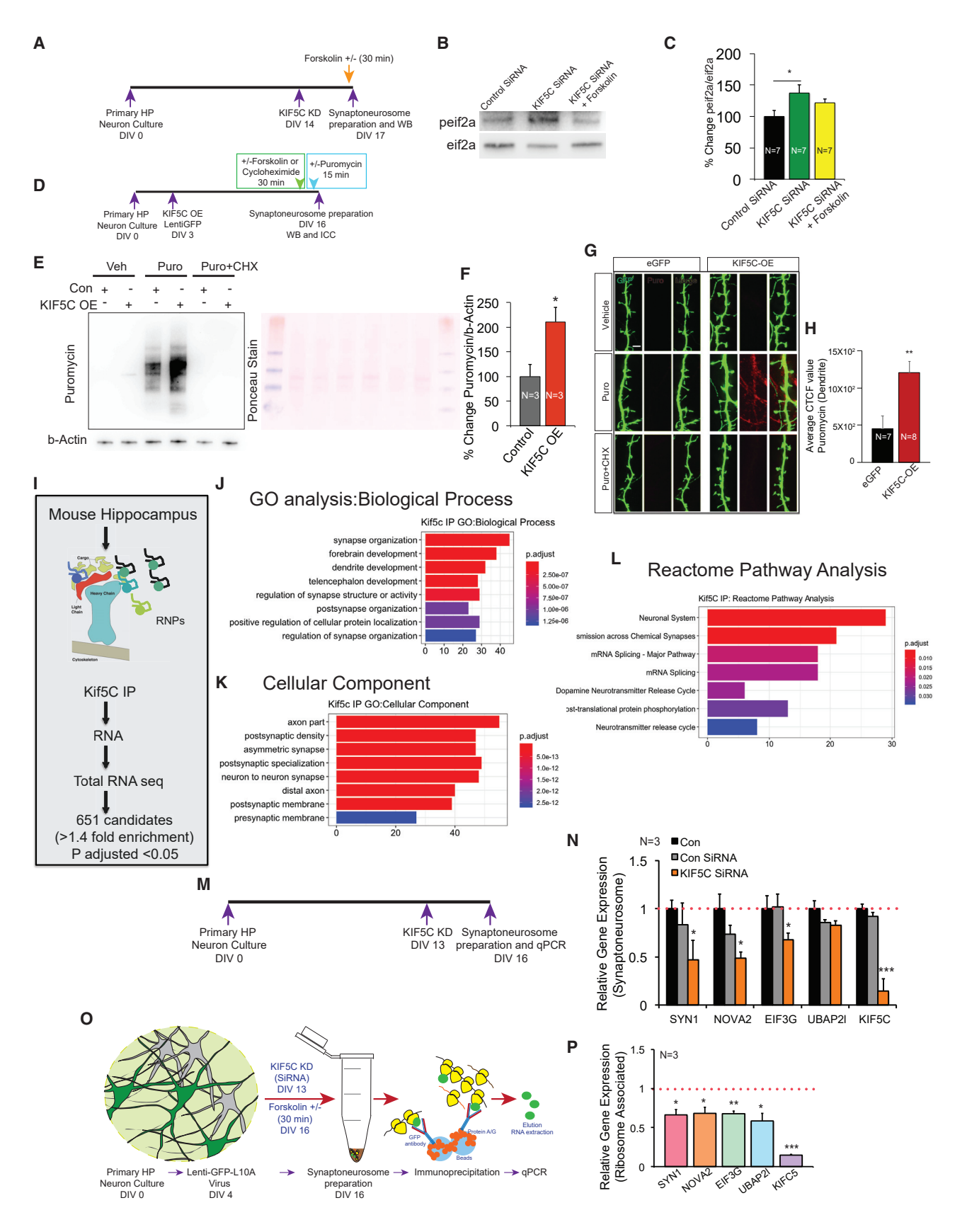
KIF5C's role mediating local translation suggests that it may transport mRNAs for translation at the synapse. RNA transport is achieved by interaction of kinesin with RNA-protein complexes (ribonucleo-particles [RNPs]). Scott et al. (2011), Puthanveettil et al. (2008), Puthanveettil (2013), and Liu et al. (2014) have shown kinesins associated with multi-protein complexes, and RNA-binding proteins are associated with distinct populations of RNAs (Kiebler and Bassell, 2006; Tübing et al., 2010; Fritzsche et al., 2013). We assumed that RNA-sequencing (RNA-seq) analysis of kinesin complexes (KIF-seq) would unravel RNAs associated with multiple RNA-binding proteins interacting with kinesin,

Figure 3. cAMP-PKA signaling regulates KIF5C expression and function

(A and B) Analysis of relative gene expression of KIF5C by quantitative real-time PCR (qPCR). RNA isolated from HP neurons after treatment with 50 μm forskolin for 30 min and 60 min ± PKA inhibitor for 30 min (B). Data normalized to 18S rRNA levels. Graphs show relative expression of KIF5C.

- (C) Experimental strategy to record mEPSCs in KIF5C KD mouse primary HP neuron cultures following exposure to forskolin or vehicle control.
- (D) Two traces of mEPSCs in ±forskolin for NC and KIF5C KD.
- (E and F) Changes in amplitudes and frequencies of mEPSCs following 72 h after KIF5C KD in ±forskolin-treated neurons. Number of neurons patched per group is labeled. Data (mean) from all KD groups compared to negative control.
- (G) Experimental strategy to record mEPSCs in mouse primary HP neuronal cultures following KIF5C OE following exposure to forskolin or vehicle control.
- (H) Two traces of mEPSCs corresponding to ±forskolin from KIF5C OE and eGFP neurons.
- (I and J) Changes in amplitudes and frequencies of mEPSCs in KIF5C OE neurons following exposure to ±forskolin. Number of neurons patched per group is labeled. Data (mean) from OE compared to control.
- (K) Experimental plan for KIF5C KD and forskolin treatment for confocal live imaging.
- (L) Confocal images showing changes in spine, digitally enlarged image in inset.
- (M and N) Quantitative analyses of image data shown in (L) executed by selecting dendrites with length of 100 μm . Graphs show change in spine density or morphology. Changes compared between KIF5C KD and NC following ±forskolin exposure. Unpaired, two-tailed Student's t test, one-way ANOVA followed by Holm-Sidak or Tukey post hoc test. Error bars represent SEM. *p < 0.05, *p < 0.005, and ***p < 0.0005. Scale bar: 20 μm.





Article



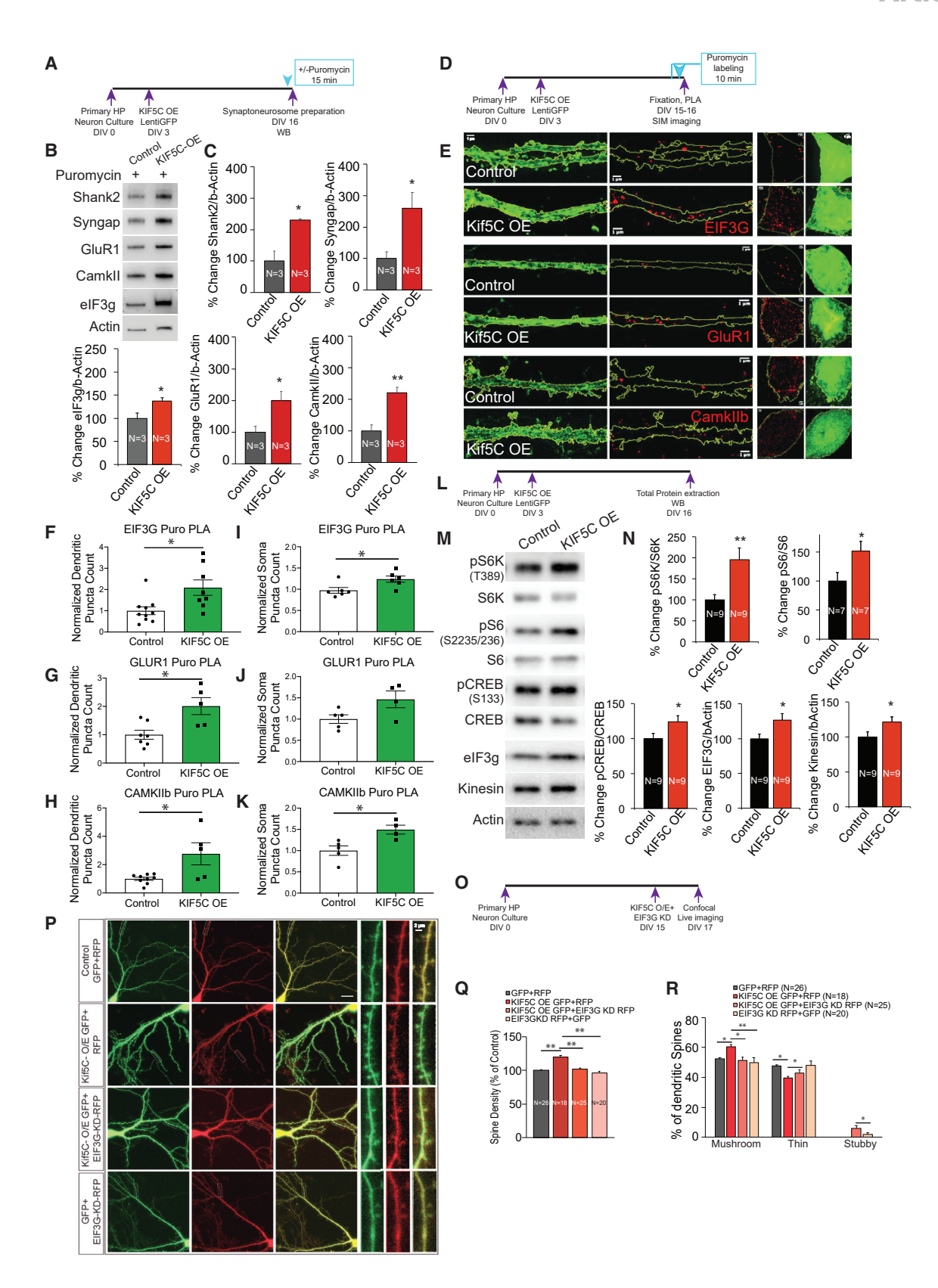
and we sought to identify KIF5C-transported RNAs by RNA-seq analysis of endogenous KIF5C complexes isolated from mouse hippocampus. Super-resolution images show endogenous KIF5C expression punctate throughout dendritic processes of matured hippocampal neurons (Figure S3L). Our KIF5C-seq analysis identified 651 coding and noncoding RNAs (>1.4-fold enrichment, p_{adjusted} < 0.05; DEseq2; Tables S2 and S3) in KIF5C coimmunoprecipitation compared with control. To identify specific signaling pathways mediated by KIF5C-transported RNAs, we analyzed RNA-seq data by Gene Ontology (GO) and Reactome pathway analysis (Figures 4I-4L; Figures S3M-S3O). We found RNAs associated with KIF5C are involved in several key synaptic pathways - synapse organization, dendritic development, axon, postsynaptic density and specializationsuggesting that KIF5C transports several synaptic-signaling RNAs. Because KIF5C-associated RNAs indicate the component of global transcriptome that is actively transported, we sought to determine whether KIF5C-associated RNAs overlap with distally localized RNAs and with global hippocampal transcriptome. We compared an RNA-seg dataset generated from neuropil of rat hippocampus (Cajigas et al., 2012), mouse hippocampus (Farris et al., 2019), and hippocampal global transcriptome (Cembrowski et al., 2016), applying the criteria: average TPM cutoff of >2; padj < 0.05, log2FoldChange > 0 (for data from Farris et al. and Cembrowski et al.). We find that KIF5Cassociated RNAs share 32% and 34.5% sequences with neuropil-localized transcriptome of rat and mouse hippocampus, respectively, and 98% with hippocampal transcriptome (Figure S3P; Tables S2, S3, and S4). Since the localized RNA pool consists of populations transported by multiple molecular motors-localized, translationally repressed, and active RNAswhereas KIF5C-associated RNAs are more dynamic, these data suggest enrichment of specific population of RNAs associated with KIF5C.

Next, we aimed to confirm whether KIF5C regulates availability of RNAs at synapse for local translation. First, focusing on 4 mRNA candidates (SYN1, UBAP21, NOVA2, EIF3G) identified from RNAseq (Table S2), we assessed whether KIF5C KD decreases expression of candidate RNAs in synaptoneurosomes. qPCR of synaptoneurosome-enriched RNAs, as well as those from cytosol fractions and total homogenates prepared from KIF5C KD or control neurons, suggested a reduction in KIF5C reduces levels of all candidate mRNAs in synaptoneurosome fractions (Figures S3Q-S3R; n = 3 for all, *p < 0.05, one-way ANOVA followed by post hoc Tukey test; Figures 4M and 4N; Table S1). Second, qPCR analysis of synaptoneurosome-associated RNAs prepared from KIF5C OE-Lenti eGFP- or control eGFP-transduced neurons showed increasing KIF5C expression upregulated levels of candidate mRNAs in homogenate and synaptoneurosomes (Figures S3S-S3T; Table S1). Third, to confirm whether KIF5C-transported RNAs are used for local translation, we expressed tagged ribosomes (L10A-eGFP-tagged ribosomes; Drane et al., 2014) in HP neurons and isolated tagged ribosomes using anti-eGFP antibody (Figures S4A and S4B). Ribosome association suggests mRNAs being translated. Total RNAs were recovered from tagged ribosomes and eGFP-alone controls, and then analyzed by Bioanalyzer to confirm integrity and expression (Figure S4C). We next isolated tagged ribosomes from forskolin-treated synaptoneurosome fractions (Figure 40). qPCR analysis of ribosomeassociated RNAs from synaptoneurosomes showed that KIF5C KD reduced levels of SYN1, UBAP21, NOVA2, and EIF3G RNA associated with ribosomes (n = 3 for all; *p < 0.05, one-way ANOVA followed by post hoc Tukey test; Figure 4P; Table S1; see also STAR Methods). Furthermore, dendritic localization these RNAs are independent of KIF3A levels (n = 6 for all; **p < 0.005, one-way ANOVA followed by post hoc Tukey test; Figure S4D; Table S1). To further confirm KIF5C-dependent RNA transport, we studied the dendritic localizations of two RNA candidates EIF3G and SYN1 in hippocampal neurons. Using structured illumination microscopy (SIM), mRNA localization was visualized using DIG-labeled antisense riboprobes for fluorescence in situ hybridization (FISH) analysis. A sense riboprobe determined specificity. Consistent with the assumption that KIF5C transports EIF3G and SYN1, we found a decrease in dendritic localization of SYN1 and EIF3G with KIF5C KD (n = 3-4 for all, *p < 0.05; unpaired, two-tailed Student's t test; Figures S4E-S4I).

Figure 4. KIF5C regulates local translation and transports RNAs critical for synapse function

- (A) Experimental strategy.
- (B) Representative WBs of pelF2α and elF2α in control, KIF5C KD, and forskolin-treated KIF5C KD synaptoneurosomes.
- (C) Normalized pelF2 α to elF2 α in three groups (B).
- (D) Experimental strategy for puromycin labeling experiment.
- (E) WB analysis of puromycin-labeled actin in KIF5C OE synaptoneurosomes from primary HP neurons treated with vehicle, puromycin (Puro), or puromycin+cycloheximide (CHX). Ponceau staining used to confirm equal loading. n = 3 independent experiments.
- (F) Normalized puromycin-labeled actin in synaptoneurosomes prepared from KIF5C OE compared with eGFP control neurons. Changes in protein synthesis compared in puromycin-treated cells. Equal loading confirmed with Ponceau staining.
- (G) SIM projection image analysis of KIF5C OE primary HP neurons treated with vehicle, Puro, or Puro+CHX. Puromycin staining shown in red. eGFP-labeled dendritic process shown in green.
- (H) Quantitative representation of average puromycin fluorescence intensity (corrected total cellular fluorescence [CTCF]) in KIF5C OE neurons in comparison to control, as observed in (G).
- (I) Experimental strategy for RNA-seq from mouse hippocampus following KIF5C IP.
- (J-L) GO analysis of KIF5C-associated RNAs showing network of genes enriched in biological processes and cellular components.
- (M) Experimental strategy for synaptoneurosome preparation.
- (N) Analysis of relative gene expression of cargos and KIF5C identified through RNA-seq in control and KIF5C KD synaptoneurosomes by qPCR.
- (O) Experimental strategy for L10A immunoprecipitation (IP) in forskolin-treated synaptoneurosomes.
- (P) Analysis of ribosome-associated relative gene expression of KIF5C-associated RNAs in control and KIF5C KD synaptoneurosomes by qPCR. For all statistical analyses, data expressed as means ± SEM (*p < 0.05, **p < 0.005, **p < 0.0005; unpaired, two-tailed Student's t test, one-way ANOVA followed by Tukey's post hoc test).





Article



EIF3G constrains structural changes induced by KIF5C

We next focused on the role of EIF3G transport in structural changes. EIF3G regulates eukaryotic translation initiation and is a major target for translational control. FISH experiments show that enhancing levels of KIF5C could increase localization of EIF3G mRNAs in dendrites (Figures S4E-S4Q). To determine whether enhancing EIF3G RNA transport indeed increases elF3g protein levels, we examined the protein levels in synaptoneurosomes isolated from KIF5C OE HP neurons. Consistent with prior data (Figures S5A-S5C; Table S1), we found KIF5C OE enhanced eIF3g protein levels in synaptoneurosomes (234.92 ± 37.60) compared to control $(100 \pm 24.60, n = 3, **p <$ 0.01; unpaired, two-tailed Student's t test; Figures S5D-S5F; Table S1). We then studied puromycin-labeled proteins isolated from synaptoneurosomes. The WB analyses in Figures 5A-5C (Table S1) show enhanced synthesis of eIF3g proteins in KIF5C OE neurons.

We questioned whether SHANK2, SYNGAP1, GLUR1, and CAMKII\(\beta\)-1—four other KIF5C RNAs—are among newly synthesized proteins due to KIF5C OE in HP neurons. Consistent with KIF5C's role in local translation, we found expression of these proteins in synaptoneurosomes is significantly enhanced with KIF5C OE(n = 3 for all, *p < 0.05, unpaired, two-tailed Student's t test; Figures 5A-5C; Table S1).

To confirm that KIF5C OE enhances translation of specific RNAs, we used the puro-PLA (puromycin-proximity ligation assay) method (Dieterich et al., 2010; tom Dieck et al., 2015) to visualize newly synthesized proteins in dendritic compartments. Following KIF5C OE at DIV 3, we executed puro-PLA at DIV 15-16 and analyzed three candidates, eIF3g, GluR1, and CamKIIβ-1 (Figures 5D-5K). Neurons transfected with GFP alone acted as controls. Consistent with prior data, KIF5C OE enhanced protein synthesis in dendrites with KIF5C OE (n = 3 for all, *p < 0.05, unpaired, two-tailed Student's t test; Figures 5F-5H; Table S1) and further confirmed that KIF5C OE enhances translation (Figure 5E). We also observed translation enhancements of eIF3g and CamKIIβ-1 in neuronal soma in KIF5C OE (n = 3 for all, *p < 0.05; unpaired, two-tailed Student's t test;

Figures 5I-5K; Table S1), suggesting KIF5C OE's global effect on translation.

We studied two other indicators of translation in KIF5C OE neurons, pS6K/S6K (phospho-S6K/total S6K) and pS6/S6 (phospho-S6/total S6), and found that pS6K and pS6 were enhanced in total protein extractions (n = 7, *p < 0.05, unpaired, two-tailed Student's t test; Figures 5L-5O; Table S1). Based on prior findings that ApKHC1 OE in Aplysia presynaptic sensory neurons (Puthanveettil et al., 2008) and KIF17 OE in mouse forebrain (Wong et al., 2002) resulted in activation of CREB-mediated transcription through feedback mechanism, we asked whether KIF5C OE could result in activation of CREB. Our WB data (Figures 5M and 5N) show that KIF5C OE (n = 9, *p < 0.05, unpaired, two-tailed Student's t test; Figures 5M and 5N; Table S1) indeed produced enhanced CREB phosphorylation, suggesting activation of CREB signaling in OE neurons (pCREB/CREB ratio: KIF5C OE: 124.02 ± 8.54 ; control: 100 ± 7.32 , n = 9).

Next, we explored EIF3G as a mediator of KIF5C OE-induced enhancement in dendritic arborization and synapse morphology. We carried out EIF3G KD by expressing EIF3G shRNAs in KIF5C OE neurons and quantified structural changes. If EIF3G levels were critical for KIF5C OE effects, EIF3G KD should inhibit structural changes in KIF5C OE neurons. We verified the extent of KD of EIF3G using two different shRNAs (Figures S5G-S5J; Table S1). Spine density measurements indicated that EIF3G knockdown in KIF5C OE neurons caused significant decrease in total spine density (n = 20, **p < 0.001, one-way ANOVA followed by post hoc Tukey test; Figures 50-5Q; Table S1).

We then analyzed spine morphology changes in KIF5C OE + EIF3G KD HP neurons, and found that EIF3G KD in the KIF5C OE neuron reduced mushroom spines compared to KIF5C OE alone. We also observed significant decrease in mushroom spines by EIF3G KD compared to KIF5C OE (mushroom spines:n = 20, *p < 0.01, one-way ANOVA followed by post hoc Tukey test; Figure 5R; Table S1).

Next, we determined dendritic arborization and, consistent with spine density and morphology data, found a significant decrease in dendritic branching in KIF5C OE + EIF3G KD neurons compared to KIF5C OE neurons (n = 14; *p < 0.01, and

Figure 5. EIF3G constrains structural changes induced by KIF5C OE

(A) Experimental strategy for puromycin labeling experiment.

- (B) WB images of Shank2, Syngap, GluR1, CamKIIβ-1, eIF3g, and actin in synaptoneurosomes prepared from KIF5C OE- or eGFP-expressing primary HP neurons treated with puromycin.
- (C) Shank2, Syngap, GluR1, CamKllβ-1, and elF3g expression levels normalized to actin in synaptoneurosomes prepared from KIF5C OE or eGFP neurons treated with puromycin.
- (D) Experimental strategy for detecting newly synthesized proteins in KIF5C OE neurons by proximity labeling assay (PLA).
- (E) Confocal images showing proximity labeling respectively for eIF3G, GluR1, and CamKIIß-1 in KIF5C OE-GFP- or eGFP-expressing primary HP neurons treated with puromycin. Newly synthesized proteins are shown in red.
- (F-H) Quantification of normalized positive puncta counts in labeled dendrites.
- (I-K) Quantification of normalized positive puncta counts in labeled soma.
- (L) Experimental strategy.
- (M) WB images of pS6K (T-389), S6K, pS6 (S235/236), S6, pCREB (S133), CREB, eIF3g, Kinesin, and actin. Primary neurons transduced with eGFP control and KIF5C OE-expressing lentiviruses. Cells lysed at DIV 16 and subjected to immunoblotting.
- (N) Normalized pS6K to S6K, pS6 to S6, pCREB to CREB, eIF3g to actin, and KIF5C to actin in total lysate of KIF5C OE- or eGFP-expressing neurons.
- (O) Experimental plan for EIF3G KD and KIF5C OE in same neuron for confocal live imaging.
- (P) Confocal projection images showing changes in spine, digitally enlarged image in inset.
- (Q and R) Quantitative analyses of image data shown in (P) completed by selecting dendrites with length of 100 μ m. Bar graphs show change in spine density or morphology. Changes compared between neurons in control and KIF5C OE groups. Unpaired, two-tailed Student's t test or one-way ANOVA followed by Tukey's or Dunnett's post hoc test. Error bars represent SEM. *p < 0.05, *p < 0.005, and ***p < 0.0005. Scale bar: 1, 2, or 20 μm .



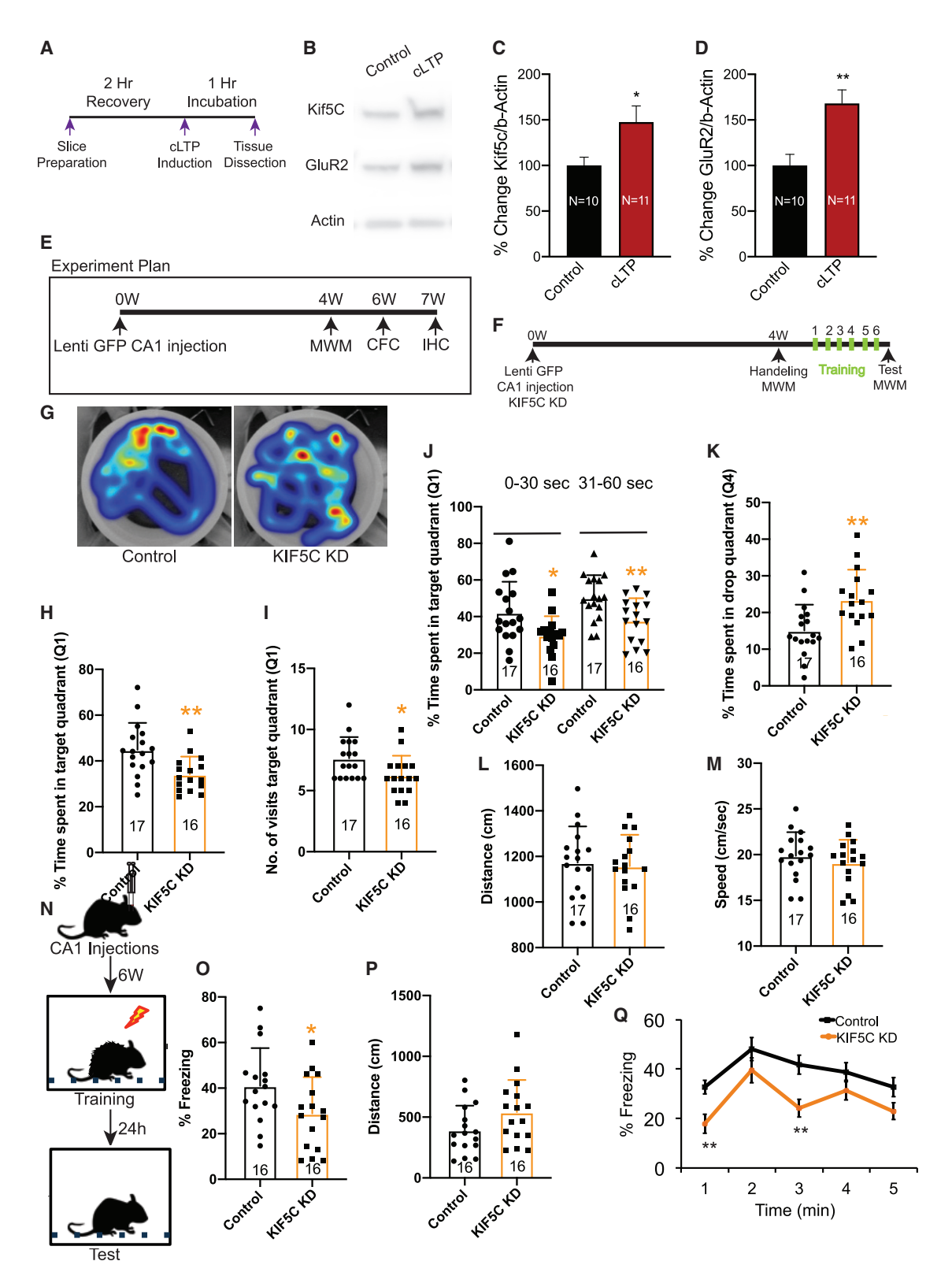


Figure 6. KIF5C expression in CA1 essential for contextual fear and spatial memories

(A) Experimental strategy followed for cLTP.

(B) WB images of Kif5C, GluR2, and Actin in CA1 after cLTP stimulation and control condition.

(C and D) Kif5C and GluR2 expression levels normalized to actin as compared to control as percentage of change.

(legend continued on next page)

Article



unpaired, two-tailed Student's t test; Figures S5K-S5M; Table S1). This suggests that KIF5C mediates local translation and structural plasticity through EIF3G localization in dendrites.

KIF5C KD in dorsal CA1 neurons produces specific learning and memory deficits in mice

The role of KIF5C in mediating dendritic and spine morphology and the regulation of its expression by cAMP signaling fueled our idea that KIF5C could be a critical component of LTM. We asked whether KIF5C expression is regulated by learning-related signaling in adult mouse hippocampus. We induced chemical LTP (cLTP) in mouse hippocampus (Ch'ng et al., 2012) and quantified KIF5C expressions by western analysis of proteins isolated from CA1 subregion. We incubated slices for 60 min in Mg²⁺-free artificial cerebrospinal fluid (ACSF) supplemented with rolipram, forskolin, and bicuculline (Kopec et al., 2006). As shown in Figures 6A and 6B, following cLTP stimulation, a robust increase in KIF5C level was detected in CA1 by immunoblotting proteins isolated from punches from the CA1 area of brain slices (n = 10; p = 0.031). A significant increase in GluR2 level with cLTP was detected by immunoblotting (p = 0.0023; unpaired, twotailed Student's t test; Figures 6C and 6D; Table S1). cLTP did not induce changes in KIF5C and GluR2 levels in other brain regions, including prefrontal cortex and striatum (n = 10; unpaired, two-tailed Student's t test; Figures S5N-S5T; Table S1). These results indicate that KIF5C protein levels are upregulated in CA1 by cLTP.

We then wondered whether manipulating KIF5C expression in CA1 by KD or OE impacted two associative memory processes-spatial memory and contextual fear memory (Figures 6E-6G; Figure S6A). Performance in Morris water maze (MWM) tested spatial memory, and contextual fear conditioning (CFC) assessed contextual fear memory.

First, we verified expression of lentiviral constructs (STAR Methods; Figures S6B-S6E). Then we studied effects of KIF5C KD on spatial memory. Control and KIF5C KD lentivirus-injected mice swam to a hidden platform (location P in quadrant Q1; Figure S6F). In the MWM, KIF5C KD virus-injected mice displayed poor spatial memory relative to control virus-injected mice (Figures 6F-6M). CA1 KIF5C KD mice also spent significantly less time in target quadrant (Q1) (34.1 \pm 1.94; n = 16) compared to control (44.9 \pm 2.8; n = 17; p = 0.0042; unpaired, two-tailed Student's t test; Figure 6H; Table S1). There were significantly fewer visits to Q1 by KIF5C KD (6.2 \pm 0.4; n = 16) compared to control $(7.7 \pm 0.42; n = 17; p = 0.022; unpaired, two-tailed Student's t$ test; Figure 6I; Table S1). Time spent in drop quadrant (Q4) by KIF5C KD also increased (23.5 \pm 2.04; n = 16) compared to control (15.1 \pm 1.7; n = 17; p = 0.003; unpaired, two-tailed Student's t test; Figure 6K; Table S1). Difference between total distances covered is comparable and similar speed was maintained during probe test (Figures 6L and 6M; Table S1). Despite improving across training, latency of CA1 KIF5C KD mice was significantly higher (Figure S6G; Table S1) than control during second, third, and fourth days of training, indicating relatively poor learning ability. The two groups maintained comparable distance and speed during training, indicating no sign of motor impairment (Figures S6H and S6I; Table S1).

We next asked whether KIF5C KD in dorsal CA1 may be critical for contextual fear memory (Figures 6N-6Q). KIF5C KD virus-injected mice (28.9 ± 3.65) displayed comparatively weaker freezing responses during retrieval than control virus-injected mice (41.03 \pm 3.8; n = 16; p = 0.043; unpaired, two-tailed Student's t test; Figure 6O; Table S1). We also examined freezing response elicited per minute and found significant reduction in freezing at the first and third minute (Figure 6Q; Table S1), while distance traveled during test was not significantly different between groups (Figure 6P; Table S1). Freezing response and distance traveled in training were comparable between groups (Figures S6J and S6K; Table S1).

Gain of function of KIF5C in dorsal CA1 neurons improves spatial memory but not contextual fear

Based on effects of KIF5C OE on excitatory synaptic transmission and mushroom spine density in neuronal cultures, we assumed that KIF5C OE could potentially enhance LTM. To test this, we studied gain of function of KIF5C by KIF5C OE in dorsal CA1 neurons on spatial and contextual fear memories (Figure 7A). First we assessed KIF5C OE in spatial memory (Figures 7B-7I). Control and KIF5C OE lentivirus-injected mice swam to a hidden platform (location P in quadrant Q1; Figure S6F). CA1 KIF5C OE mice spent significantly more time (43.9 ± 3.3) in the platform-containing quadrant than controls (32.5 ± 2.4) during probe trial on day 7 (p value, 0.01; Figure 7D; Table S1), suggesting spatial memory improvement. Number of visits to Q1 was comparable between CA1 KIF5C OE mice (7.8 \pm 0.4) and controls (7.9 \pm 0.7; Figure 7E; Table S1). Time spent in Q4 was comparable between KIF5C OE mice (18.13 \pm 2.04) and controls (20.96 ± 3.1; Figure 7G; Table S1). Control and CA1 KIF5C OE mice did not differ in escape latencies on days of training (Figure S6L; Table S1). Similar speed was maintained during probe test in CA1 KIF5C OE mice (19.4 \pm 0.65) and controls (19.8 \pm 0.77). Moreover, distance traveled by KIF5C OE mice (1208.7 \pm 40.5) was comparable to controls (1,256.4 \pm 52.3), suggesting no motor or visual impairment (Figures 7H and 7I; Figures S6M and S6N; Table S1).

⁽E) Experimental strategy for in vivo manipulation and mouse behavior using lentivirus to KD KIF5C expression.

⁽F) MWM test strategy.

⁽G) Heatmap showing mouse tracking during MWM.

⁽H-M) Performance in MWM. (H) Time spent in Q1 during probe test. (I) Total number of visits to Q1 during probe test. (J) Time spent every 30 s in Q1 during probe test. (K) Time spent in Q4 during probe test. (L) Total distance traveled during probe test. (M) Swimming velocity.

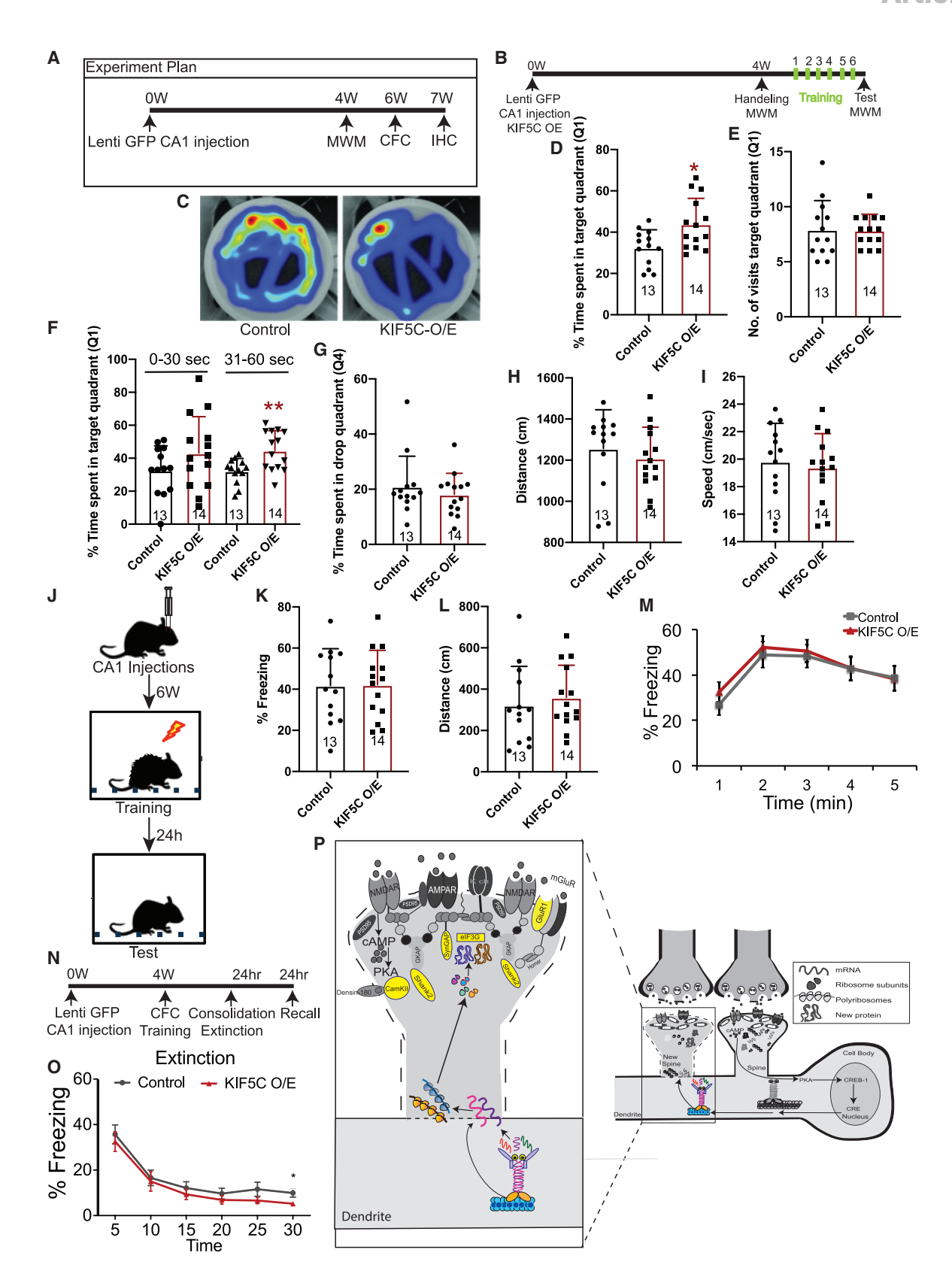
⁽N) Contextual fear memory test strategy.

⁽O) Contextual freezing responses during test at 24 h after conditioning.

⁽P) Total distance traveled during test at 24 h after conditioning.

⁽Q) Mean percentage freezing time-averaged every minute during 5-min test at 24 h after conditioning. For all statistical analyses, data expressed as means ± SEM (*p < 0.05, **p < 0.05; unpaired, two-tailed Student's t test).





Article



In contrast to spatial memory, we observed no enhancements to contextual fear memory (Figure 7J). Percent freezing measured at 24 h after training in KIF5C OE (42.2 \pm 4.5) lentivirus-injected mice and controls were not significantly different (41.8 \pm 5.0, 24 h after foot shock; Figures 7K-7M; Figure S6O and S6P; Table S1).

Our results suggest that KIF5C OE effects are selective exclusively for spatial memory, but we speculated that lack of effect on contextual fear could be due to the strong shock paradigm used during training, masking potential memory enhancements due to ceiling effect. We applied a lower-intensity foot shock paradigm (Figure 7N) and assessed two other fear memoryrelated paradigms, extinction of contextual fear and extinction recall. We examined percent freezing after foot shock in each session: habituation (KIF5C OE: 0.16 \pm 0.06, n = 9; control: 0.33 ± 0.30 , n = 11), session 1 (KIF5C OE: 1.25 ± 0.46 , n = 9; control: 1.42 ± 0.70 , n = 11), session 2 (KIF5C OE: 7.65 ± 2.0 , n = 9; control: 10.27 \pm 1.72, n = 11), and session 3 (KIF5C OE: 8.59 \pm 3.39, n = 9; control: 6.8 ± 2.32 , n = 11). We observed percent change in freezing was comparable in control and KIF5C OE mice (Figure S6Q). Next, we examined whether training exposure induces generalization in KIF5C OE mice. We found the percent freezing per minute bin: min1 (KIF5C OE: 16.2 ± 2.72, n = 9; control: 27.44 \pm 4.62, n = 11), min2 (KIF5C OE: 41.43 \pm 5.06, n = 9; control: 45.0 ± 5.25 , n = 11), min3 (KIF5C OE: 38.27 ± 6.77 , n = 9; control: 37.71 ± 6.01 , n = 11), min4 (KIF5C OE: 35.66 ± 5.08 , n = 9; control: 40.8 ± 6.16 , n = 11), and min5 (KIF5C OE: 30.9 ± 7.17 , n = 9; control: 27.34 ± 6.0 , n = 11). No significant difference in consolidation of fear memory between control and KIF5C overexpressed mice appeared (Figure S6R).

Given that extinction trace decays over time, we tested fear memories for 30 min, tracking every 5 min (Table S1). We observed enhanced extinction of contextual fear in KIF5C OE mice (at 30 min, *p = 0.0497; Figure 70). When control and KIF5C OE mice were assessed for extinction recall, freezing performance was comparable every minute for 5-min test among groups (Figure S6S; Table S1), suggesting KIF5C OE enhances extinction and does not impact consolidation or extinction recall of contextual fear memory.

Next, we examined whether the effects of KIF5C manipulation produced structural changes in vivo, similar to primary HP neurons (Figure S6T). Consistent with in vitro data, total spine density in CA1 neurons decreased with KIF5C KD but increased with KIF5C OE compared to eGFP control (*p = 0.01, one-way ANOVA followed by post hoc Dunnett's test; Figure S6U; Table S1). Our analysis showed significant reduction in mushroom spines in KIF5C KD CA1 neurons and increase in mushroom spines in KIF5C OE CA1 neurons compared to control (*p < 0.01, one-way ANOVA followed by post hoc Dunnett's test; Figure S6V; Table S1).

DISCUSSION

Our aim in this work was to assess the role of Kif mediated longdistance transport in structural plasticity and memory. We studied contributions of KIF5C and KIF3A expressed in the same HP neurons (Liu et al., 2014) in excitatory synaptic transmission, spine density, morphology, and dendritic arborization. While both Kifs are critical for synaptic transmission and morphology, only KIF5C OE enhanced mEPSCs and structural plasticity in HP neurons.

Regulation of local translation by KIF5C-mediated transport of RNAs

Identification of localized RNAs provides important clues to local protein synthesis and informs us of proteins needed at synapse for structural plasticity associated with memory storage. Aplysia studies have identified several RNAs localized to sensory neuron terminals (Moccia et al., 2003; Moroz et al., 2006) and a molecular motor (ApKHC1) that mediates the transport of RNAs to neuronal terminals (Puthanveettil, 2013). Microarray and RNA-seg methodologies successfully identified several RNAs localized to mammalian neuronal dendrites (Kim et al., 2004; Sambandan et al., 2017), but Kifs involved in dendritic localization remain elusive. In mouse neurons, several RNA binding proteins have been associated with the tail domain of KIF5C (Kanai et al., 2004), suggesting a role for KIF5C-mediated transport of RNAs to dendrites. As structural changes at the synapse require local new protein synthesis, we considered that KIF5C might transport RNAs to dendrites for local translation. KIF5C KD decreased density of mushroom spines, whereas its OE enhanced it. Consistent with our assumption that KIF5C OE might enhance translation to produce structural

Figure 7. KIF5C OE in dorsal CA1 improves spatial memory and extinction of contextual fear memory but not consolidation or recall

(A) Experimental strategy for in vivo manipulation and mouse behavior using lentivirus to overexpress KIF5C.

- (B) MWM test strategy.
- (C) Heatmap showing mouse tracking during MWM.
- (D-I) MWM performance. (D) Time spent in Q1 during probe test. (E) Total visits to Q1 during probe test. (F) Time spent every 30 s in Q1 during probe test. (G) Time spent in Q4 during probe test. (H) Total distance traveled during probe test. (I) Swimming velocity during test.
- (J) Contextual fear memory test strategy.
- (K) Contextual freezing responses during test at 24 h after conditioning.
- (L) Total distance traveled during test at 24 h after conditioning.
- (M) Mean percentage freezing time-averaged every minute during 5 min test at 24 h after conditioning.
- (N) Experimental strategy for assessing consolidation, extinction, and recall of contextual fear in CA1 KIF5C OE mice using reduced-intensity foot shocks during
- (O) Extinction training shows significant reduction in percent freezing at 30 min. Control, n = 11; KIF5C-O/E, n = 9. For all statistical analyses, data expressed as means ± SEM (*p < 0.05, **p < 0.05; unpaired, two-tailed Student's t test).
- (P) KIF5C functions as critical regulator of structural plasticity associated with LTM, linking transcription, transport, and local translation. KIF5C mediates longdistance transport of RNA substrates for local translation for learning-related synaptic remodeling. EIF3G, regulator of eukaryotic translational initiation, and several key components determining plasticity and function of excitatory synapses such as GLUR1, SYNGAP, SHANK2, and CaMKII-β, are transported as RNA cargo of KIF5C.





changes at the synapse, we find from puromycin labeling experiments that KIF5C OE resulted in enhanced translation.

To identify populations of RNAs transported by KIF5C, we developed KIF-seq, isolating endogenous KIF5C complexes by coimmunoprecipitation (co-IP) from hippocampal neurons and analyzing components by RNA-seq. We identified ~650 RNAs (p_{adi} < 0.05) associated with KIF5C. These RNAs are involved in synapse function, protein synthesis, and neurodegenerative disorders. They may serve as substrates for local new protein synthesis (Figure 7P), suggesting a key role for KIF5C in dendritic RNA localization in HP neurons—as KIF5C function could determine availability of these RNAs for local translation.

We found that synaptic localization of RNAs encoding key proteins involved in plasticity and memory, such as GLUR1, SYN-GAP, SHANK2, and $CAMKII\beta$ -1, is mediated by KIF5C (Figure 7P). These RNAs encode critical components of translational machinery and excitatory synapse. Taken together KIF5C-mediated transport is a key regulatory mechanism linking transcription, local protein synthesis, and structural plasticity in HP neurons.

KIF5C as key regulator of structural plasticity and LTM

Only a few genetic studies exist on loss of function of Kifs in LTM (Kondo et al., 2012; Muhia et al., 2016; Yin et al., 2011; Muhia et al., 2016; Makrythanasis et al., 2018; Zhao et al., 2020), and no exploration of kinesin OE in specific subregions of mammalian brain on memory and learning has been undertaken. Our imaging, electrophysiology, and molecular experiments described in Figures 1, 2, 3, 4, and 5 suggest that KIF5C is a key regulator of structural plasticity in cultured HP neurons. Consistent with these observations, we find that KIF5C levels in hippocampal CA1 neurons are regulated by neuronal activity and altering KIF5C levels produce a corresponding change in spine density and morphology of CA1 neurons.

Next, we asked whether KIF5C-mediated long-distance transport in CA1 impacts different memories. We studied effects of KIF5C manipulation in CA1 neurons in spatial memory and contextual fear memory. We find that KIF5C depletion in CA1 interferes with encoding and retrieval of spatial memory as well as impairing contextual fear memory (Figure 6). These data indicate that restricted, post-developmental KD of KIF5C expression in CA1 impairs both spatial and fear memory, illustrating the significance of KIF5C-mediated long-distance transport in multiple forms of LTM.

KIF5C OE in CA1 improved mouse performance in the spatial memory task but did not enhance contextual fear memory, although we employed fear conditioning using reduced shock and executed multiple fear-related behavior assays. Training at reduced intensity did not show enhancements in contextual fear but did show enhancements in fear extinction. Extinction recall memory was not affected. These results suggest cargos transported by KIF5C may have memory-specific functions. It is possible that in CA1 neurons of KIF5C OE mice, levels in KIF5C-mediated long-distance transport required to improve contextual fear memory were not achieved, whereas those required to enhance spatial memory were; or, because spatial and contextual memory recruit different neural circuits involving CA1, enhancements in KIF5C function in CA1 alone may be insufficient to enhance contextual fear memory.

Its been shown previously that gain of function of specific genes improves memory. Tang et al., (1999) reported enhancement of memory after OE of NR2B using transgenic mouse model, whereas OE of adeno-associated virus (AAV) vector expressing alphaCaMKII improved spatial memory (Poulsen et al., 2007). Transgenic mice overexpressing KIF17 improved spatial memory (Wong et al., 2002). Here, we find that restricted manipulation of KIF5C in CA1 neurons specifically constrains multiple memory processes. Consistent with prior findings that gain of function of kinesin results in activation of CREB, we find that KIF5C OE results in activation of CREB and enhances translation. KIF5C OE enhances delivery of synaptic cargos, leading to activation of synaptic signaling pathways. This synaptic activation produces several changes, including those in regulators of translation and transcription (Figures 5D-5F), ultimately producing structural changes.

Our study demonstrating that KIF5C-mediated long-distance transport of RNAs links local translation and structural plasticity is a previously unrecognized mechanism of LTM. These findings lay a foundation in the search for mechanistic relationships between temporal changes in transport and local translation, as determinants of activity-dependent changes in structural plasticity impacting LTM.

STAR*METHODS

Detailed methods are provided in the online version of this paper and include the following:

- KEY RESOURCES TABLE
- RESOURCE AVAILABILITY
 - Lead contact
 - Materials availability
 - Data and code availability
- EXPERIMENTAL MODEL AND SUBJECT DETAILS
 - HEK293 cell culture
- METHODS DETAILS
 - Neuronal cell cultures
 - Constructs and transfection
 - Measurements of mEPSCs
 - Live imaging
 - Characterization of KIF5C and KIF3A overexpression (OE) plasmids
 - Overexpression of KIF5C and knockdown of KIF3A in the same neurons
 - O Immunocytochemistry (ICC) and fluorescence in situ hybridization (FISH) analysis
 - KIF5C coimmunoprecipitation (CoIP), RNA-Seq and bioinformatics analysis
 - O Structured illumination super-resolution microscopy (SIM)
 - Characterization of synaptoneurosomes
 - Optimization of puromycin labeling of newly synthesized proteins
 - Puro-proximity ligation assay (PLA)
 - Synaptic protein extraction and western blotting
 - Synaptic protein extraction and immunoprecipitation
 - RNA isolation, reverse transcription and qRT-PCR

Article



- Chemical long-term potentiation (cLTP)
- Preparation of lentiviral vectors
- Characterization of lentiviral vectors
- Stereotaxic injections
- Behavioral tests
- Morris water maze (MWM)
- Contextual fear conditioning (CFC)
- Histological analysis
- Statistics
- QUANTIFICATION AND STATISTICAL ANALYSIS

SUPPLEMENTAL INFORMATION

Supplemental information can be found online at https://doi.org/10.1016/j. celrep.2021.109369.

ACKNOWLEDGMENTS

We gratefully acknowledge funding support from NIH (5R01MH094607-05 and 5R21MH108929-02), NSF (Award number 1453799), and a Training Grant in Alzheimer's Drug Discovery from the Lottie French Lewis Fund of the Community Foundation for Palm Beach and Martin Counties, Florida, enabling us to carry out this work; Dr. Long Yan of Max Planck Florida Institute (MPFI) for Neuroscience for troubleshooting confocal imaging and analyses; Dr. Vidhya Rangaraju for troubleshooting PLA experiments; and Drs. Pabalu Karunadharma and Adrian Reich, Scripps Research for RNAseq and Bioinformatics Analysis. We are grateful to Kathleen O'Brien, Scripps Florida, for carefully editing the manuscript. Furthermore, we thank the anonymous reviewers whose suggestions helped us in enhancing our manuscript.

AUTHOR CONTRIBUTIONS

Conceptualization, S.V.P. and S.S.; methodology and data analysis, S.S., Y.A., I.E., E.G., X.-a.L., and B.L.R.; performance of CA1 injections, A.Z.; generation of lentiviral vectors, S.M.; preparation of FISH probes, A.S.; investigation, S.V.P. and S.S.; writing and editing, S.V.P. and S.S. with input from all authors; supervision, S.V.P. (overall), K.M. (FRAP), S.V. (lentiviral prep), and D.P. (CA1 injections).

DECLARATION OF INTERESTS

The authors declare no competing interests.

Received: June 17, 2020 Revised: February 16, 2021 Accepted: June 18, 2021 Published: July 13, 2021

REFERENCES

Alberini, C.M., Ghirardi, M., Metz, R., and Kandel, E.R. (1994). C/EBP is an immediate-early gene required for the consolidation of long-term facilitation in Aplysia. Cell 76, 1099-1114.

Bacskai, B.J., Hochner, B., Mahaut-Smith, M., Adams, S.R., Kaang, B.K., Kandel, E.R., and Tsien, R.Y. (1993). Spatially resolved dynamics of cAMP and protein kinase A subunits in Aplysia sensory neurons. Science 260, 222–226.

Banker, G., and Goslin, K. (1988). Developments in neuronal cell culture. Nature 336, 185-186.

Bekinschtein, P., Cammarota, M., Katche, C., Slipczuk, L., Rossato, J.I., Goldin, A., Izquierdo, I., and Medina, J.H. (2008). BDNF is essential to promote persistence of long-term memory storage. Proc. Natl. Acad. Sci. USA 105, 2711-2716.

Bie, B., and Pan, Z.Z.Z. (2005). Increased glutamate synaptic transmission in the nucleus raphe magnus neurons from morphine-tolerant rats. Mol. Pain 1, 7. Burgos-Robles, A., Vidal-Gonzalez, I., and Quirk, G.J. (2009). Sustained conditioned responses in prelimbic prefrontal neurons are correlated with fear expression and extinction failure. J. Neurosci. 29, 8474-8482.

Cajigas, I.J., Tushev, G., Will, T.J., tom Dieck, S., Fuerst, N., and Schuman, E.M. (2012). The local transcriptome in the synaptic neuropil revealed by deep sequencing and high-resolution imaging. Neuron 74, 453-466.

Cembrowski, M.S., Wang, L., Sugino, K., Shields, B.C., and Spruston, N. (2016). Hipposeq: a comprehensive RNA-seq database of gene expression in hippocampal principal neurons. eLife 5, e14997.

Ch'ng, T.H., Uzgil, B., Lin, P., Avliyakulov, N.K., O'Dell, T.J., and Martin, K.C. (2012). Activity-dependent transport of the transcriptional coactivator CRTC1 from synapse to nucleus. Cell 150, 207-221.

Chen, C., and Regehr, W.G. (1997). The mechanism of cAMP-mediated enhancement at a cerebellar synapse. J. Neurosci. 17, 8687-8694.

Costa-Mattioli, M., Gobert, D., Harding, H., Herdy, B., Azzi, M., Bruno, M., Bidinosti, M., Ben Mamou, C., Marcinkiewicz, E., Yoshida, M., et al. (2005). Translational control of hippocampal synaptic plasticity and memory by the el-F2alpha kinase GCN2. Nature 436, 1166-1173.

Cover, K.K., Maeng, L.Y., Lebrón-Milad, K., and Milad, M.R. (2014). Mechanisms of estradiol in fear circuitry: implications for sex differences in psychopathology. Transl. Psychiatry 4, e422.

Davis, R.L. (2011). Traces of Drosophila memory. Neuron 70, 8-19.

Dictenberg, J.B., Swanger, S.A., Antar, L.N., Singer, R.H., and Bassell, G.J. (2008). A direct role for FMRP in activity-dependent dendritic mRNA transport links filopodial-spine morphogenesis to fragile X syndrome. Dev. Cell 14,

Dieterich, D.C., Hodas, J.J., Gouzer, G., Shadrin, I.Y., Ngo, J.T., Triller, A., Tirrell, D.A., and Schuman, E.M. (2010). In situ visualization and dynamics of newly synthesized proteins in rat hippocampal neurons. Nat. Neurosci. 13, 897-905.

Drane, L., Ainsley, J.A., Mayford, M.R., and Reijmers, L.G. (2014). A transgenic mouse line for collecting ribosome-bound mRNA using the tetracycline transactivator system. Front. Mol. Neurosci. 7, 82.

Farris, S., Ward, J.M., Carstens, K.E., Samadi, M., Wang, Y., and Dudek, S.M. (2019). Hippocampal subregions express distinct dendritic transcriptomes that reveal differences in mitochondrial function in CA2. Cell Rep. 29, 522-

Fioriti, L., Myers, C., Huang, Y.Y., Li, X., Stephan, J.S., Trifilieff, P., Colnaghi, L., Kosmidis, S., Drisaldi, B., Pavlopoulos, E., and Kandel, E.R. (2015). The persistence of hippocampal-based memory requires protein synthesis mediated by the prion-like protein CPEB3. Neuron 86, 1433–1448.

Franklin, K.B.J., and Paxinos, G.T. (1996). The Mouse Brain in Stereotaxic Coordinates (Academic Press).

Fritzsche, R., Karra, D., Bennett, K.L., Ang, F.Y., Heraud-Farlow, J.E., Tolino, M., Doyle, M., Bauer, K.E., Thomas, S., Planyavsky, M., et al. (2013). Interactome of two diverse RNA granules links mRNA localization to translational repression in neurons. Cell Rep. 5, 1749-1762.

Fykse, E.M., Takei, K., Walch-Solimena, C., Geppert, M., Jahn, R., De Camilli, P., and Südhof, T.C. (1993). Relative properties and localizations of synaptic vesicle protein isoforms: the case of the synaptophysins. J. Neurosci. 13, 4997-5007.

Hayashi, K., Suzuki, A., Hirai, S., Kurihara, Y., Hoogenraad, C.C., and Ohno, S. (2011). Maintenance of dendritic spine morphology by partitioning-defective 1b through regulation of microtubule growth. J. Neurosci. 31, 12094–12103.

Hirokawa, N., Noda, Y., Tanaka, Y., and Niwa, S. (2009). Kinesin superfamily motor proteins and intracellular transport. Nat. Rev. Mol. Cell Biol. 10, 682-696.

Hulsen, T., de Vlieg, J., and Alkema, W. (2008). BioVenn—a web application for the comparison and visualization of biological lists using area-proportional Venn diagrams. BMC Genomics 9, 488.

Kadakkuzha, B.M., Liu, X.A., McCrate, J., Shankar, G., Rizzo, V., Afinogenova, A., Young, B., Fallahi, M., Carvalloza, A.C., Raveendra, B., and Puthanveettil, S.V. (2015). Transcriptome analyses of adult mouse brain reveal enrichment of



IncRNAs in specific brain regions and neuronal populations. Front. Cell. Neurosci 9 63

Kanai, Y., Dohmae, N., and Hirokawa, N. (2004). Kinesin transports RNA: isolation and characterization of an RNA-transporting granule. Neuron 43, 513-525.

Kandel, E.R. (2012). The molecular biology of memory: cAMP, PKA, CRE, CREB-1, CREB-2, and CPEB. Mol. Brain 5, 14.

Kiebler, M.A., and Bassell, G.J. (2006). Neuronal RNA granules: movers and makers. Neuron 51, 685-690.

Kim, J., Krichevsky, A., Grad, Y., Hayes, G.D., Kosik, K.S., Church, G.M., and Ruvkun, G. (2004). Identification of many microRNAs that copurify with polyribosomes in mammalian neurons. Proc. Natl. Acad. Sci. USA 101, 360-365.

Kondo, M., Takei, Y., and Hirokawa, N. (2012). Motor protein KIF1A is essential for hippocampal synaptogenesis and learning enhancement in an enriched environment. Neuron 73, 743-757.

Kopec, C.D., Li, B., Wei, W., Boehm, J., and Malinow, R. (2006). Glutamate receptor exocytosis and spine enlargement during chemically induced longterm potentiation. J. Neurosci. 26, 2000-2009.

Kwak, J.E., Drier, E., Barbee, S.A., Ramaswami, M., Yin, J.C., and Wickens, M. (2008). GLD2 poly(A) polymerase is required for long-term memory. Proc. Natl. Acad Sci USA 105 14644-14649

Lebrón-Milad, K., Tsareva, A., Ahmed, N., and Milad, M.R. (2013). Sex differences and estrous cycle in female rats interact with the effects of fluoxetine treatment on fear extinction. Behav. Brain Res. 253, 217-222.

Liu, X.A., Kadakkuzha, B., Pascal, B., Steckler, C., Akhmedov, K., Yan, L., Chalmers, M., and Puthanveettil, S.V. (2014). New approach to capture and characterize synaptic proteome. Proc. Natl. Acad. Sci. USA 111, 16154-16159.

Livak, K.J., and Schmittgen, T.D. (2001). Analysis of relative gene expression data using real-time quantitative PCR and the 2(-Delta Delta C(T)) method. Methods 25, 402-408.

Lyons, D.A., Naylor, S.G., Scholze, A., and Talbot, W.S. (2009). Kif1b is essential for mRNA localization in oligodendrocytes and development of myelinated axons. Nat. Genet. 41, 854-858.

Ma, N., Abel, T., and Hernandez, P.J. (2009). Exchange protein activated by cAMP enhances long-term memory formation independent of protein kinase A. Learn. Mem. 16, 367-370.

Mahmmoud, R.R., Sase, S., Aher, Y.D., Sase, A., Gröger, M., Mokhtar, M., Höger, H., and Lubec, G. (2015). Spatial and working memory is linked to spine density and mushroom spines. PLoS ONE 10, e0139739.

Makrythanasis, P., Maroofian, R., Stray-Pedersen, A., Musaev, D., Zaki, M.S., Mahmoud, I.G., Selim, L., Elbadawy, A., Jhangiani, S.N., Coban Akdemir, Z.H., et al. (2018). Biallelic variants in KIF14 cause intellectual disability with microcephaly. Eur. J. Hum. Genet. 26, 330-339.

Marquèze-Pouey, B., Wisden, W., Malosio, M.L., and Betz, H. (1991). Differential expression of synaptophysin and synaptoporin mRNAs in the postnatal rat central nervous system. J. Neurosci. 11, 3388-3397.

Martin, K.C., Michael, D., Rose, J.C., Barad, M., Casadio, A., Zhu, H., and Kandel, E.R. (1997). MAP kinase translocates into the nucleus of the presynaptic cell and is required for long-term facilitation in Aplysia. Neuron 18, 899–912.

Miniaci, M.C., Kim, J.H., Puthanveettil, S.V., Si, K., Zhu, H., Kandel, E.R., and Bailey, C.H. (2008). Sustained CPEB-dependent local protein synthesis is required to stabilize synaptic growth for persistence of long-term facilitation in Aplysia. Neuron 59, 1024-1036.

Moccia, R., Chen, D., Lyles, V., Kapuya, E., e, Y., Kalachikov, S., Spahn, C.M., Frank, J., Kandel, E.R., Barad, M., and Martin, K.C. (2003). An unbiased cDNA library prepared from isolated Aplysia sensory neuron processes is enriched for cytoskeletal and translational mRNAs. J. Neurosci. 23, 9409-9417.

Morikawa, M., Tanaka, Y., Cho, H.S., Yoshihara, M., and Hirokawa, N. (2018). The molecular motor KIF21B mediates synaptic plasticity and fear extinction by terminating Rac1 activation. Cell Rep. 23, 3864-3877.

Moroz, L.L., Edwards, J.R., Puthanveettil, S.V., Kohn, A.B., Ha, T., Heyland, A., Knudsen, B., Sahni, A., Yu, F., Liu, L., et al. (2006). Neuronal transcriptome of Aplysia: neuronal compartments and circuitry. Cell 127, 1453-1467.

Muhia, M., Thies, E., Labonté, D., Ghiretti, A.E., Gromova, K.V., Xompero, F., Lappe-Siefke, C., Hermans-Borgmeyer, I., Kuhl, D., Schweizer, M., et al. (2016). The kinesin KIF21B regulates microtubule dynamics and is essential for neuronal morphology, synapse function, and learning and memory. Cell Rep. 15, 968-977.

Nakayama, K., Ohashi, R., Shinoda, Y., Yamazaki, M., Abe, M., Fujikawa, A., Shigenobu, S., Futatsugi, A., Noda, M., Mikoshiba, K., et al. (2017). RNG105/caprin1, an RNA granule protein for dendritic mRNA localization, is essential for long-term memory formation. eLife 6, e29677.

Nangaku, M., Sato-Yoshitake, R., Okada, Y., Noda, Y., Takemura, R., Yamazaki, H., and Hirokawa, N. (1994). KIF1B, a novel microtubule plus enddirected monomeric motor protein for transport of mitochondria. Cell 79, 1209-1220.

O'Brien, R.J., Kamboj, S., Ehlers, M.D., Rosen, K.R., Fischbach, G.D., and Huganir, R.L. (1998). Activity-dependent modulation of synaptic AMPA receptor accumulation. Neuron 21, 1067-1078.

Ohashi, S., Koike, K., Omori, A., Ichinose, S., Ohara, S., Kobayashi, S., Sato, T.A., and Anzai, K. (2002). Identification of mRNA/protein (mRNP) complexes containing Puralpha, mStaufen, fragile X protein, and myosin Va and their association with rough endoplasmic reticulum equipped with a kinesin motor. J. Biol. Chem. 277, 37804-37810.

Ortiz, O., Delgado-García, J.M., Espadas, I., Bahí, A., Trullas, R., Dreyer, J.L., Gruart, A., and Moratalla, R. (2010). Associative learning and CA3-CA1 synaptic plasticity are impaired in D1R null, Drd1a-/- mice and in hippocampal siRNA silenced Drd1a mice. J. Neurosci. 30, 12288-12300.

Pai, T.P., Chen, C.C., Lin, H.H., Chin, A.L., Lai, J.S., Lee, P.T., Tully, T., and Chiang, A.S. (2013). Drosophila ORB protein in two mushroom body output neurons is necessary for long-term memory formation. Proc. Natl. Acad. Sci. USA 110, 7898-7903.

Poulsen, D.J., Standing, D., Bullshields, K., Spencer, K., Micevych, P.E., and Babcock, A.M. (2007). Overexpression of hippocampal Ca2+/calmodulindependent protein kinase II improves spatial memory. J. Neurosci. Res. 85,

Puthanveettil, S.V. (2013). RNA transport and long-term memory storage. RNA Biol. 10, 1765-1770.

Puthanveettil, S.V., Monje, F.J., Miniaci, M.C., Choi, Y.B., Karl, K.A., Khandros. E., Gawinowicz, M.A., Sheetz, M.P., and Kandel, E.R. (2008). A new component in synaptic plasticity: upregulation of kinesin in the neurons of the gillwithdrawal reflex. Cell 135, 960-973.

Rao, A., Kim, E., Sheng, M., and Craig, A.M. (1998). Heterogeneity in the molecular composition of excitatory postsynaptic sites during development of hippocampal neurons in culture. J. Neurosci. 18, 1217-1229.

Raveendra, B.L., Swarnkar, S., Avchalumov, Y., Liu, X.A., Grinman, E., Badal, K., Reich, A., Pascal, B.D., and Puthanveettil, S.V. (2018). Long noncoding RNA GM12371 acts as a transcriptional regulator of synapse function. Proc. Natl. Acad. Sci. USA 115, E10197-E10205.

Ravi, V., Jain, A., Ahamed, F., Fathma, N., Desingu, P.A., and Sundaresan, N.R. (2018). Systematic evaluation of the adaptability of the non-radioactive SUnSET assay to measure cardiac protein synthesis. Sci. Rep. 8, 4587.

Rizzo, V., Touzani, K., Raveendra, B.L., Swarnkar, S., Lora, J., Kadakkuzha, B.M., Liu, X.A., Zhang, C., Betel, D., Stackman, R.W., and Puthanveettil, S.V. (2017). Encoding of contextual fear memory requires de novo proteins in the prelimbic cortex. Biol. Psychiatry Cogn. Neurosci. Neuroimaging 2,

Rui, Y., Myers, K.R., Yu, K., Wise, A., De Blas, A.L., Hartzell, H.C., and Zheng, J.Q. (2013). Activity-dependent regulation of dendritic growth and maintenance by glycogen synthase kinase 3β. Nat. Commun. 4, 2628.

Sambandan, S., Akbalik, G., Kochen, L., Rinne, J., Kahlstatt, J., Glock, C., Tushev, G., Alvarez-Castelao, B., Heckel, A., and Schuman, E.M. (2017).

Article



Activity-dependent spatially localized miRNA maturation in neuronal dendrites. Science 355, 634-637.

Scott, D.A., Das, U., Tang, Y., and Roy, S. (2011). Mechanistic logic underlying the axonal transport of cytosolic proteins. Neuron 70, 441–454.

Sekine, Y., Okada, Y., Noda, Y., Kondo, S., Aizawa, H., Takemura, R., and Hirokawa, N. (1994). A novel microtubule-based motor protein (KIF4) for organelle transports, whose expression is regulated developmentally. J. Cell Biol. 127, 187-201.

Sharifnia, P., and Jin, Y. (2015). Regulatory roles of RNA binding proteins in the nervous system of C. elegans. Front. Mol. Neurosci. 7, 100.

Tang, Y.P., Shimizu, E., Dube, G.R., Rampon, C., Kerchner, G.A., Zhuo, M., Liu, G., and Tsien, J.Z. (1999). Genetic enhancement of learning and memory in mice. Nature 401, 63-69.

tom Dieck, S., Kochen, L., Hanus, C., Heumüller, M., Bartnik, I., Nassim-Assir, B., Merk, K., Mosler, T., Garg, S., Bunse, S., et al. (2015). Direct visualization of newly synthesized target proteins in situ. Nat. Methods 12, 411-414.

Tsutajima, J., Kunitake, T., Wakazono, Y., and Takamiya, K. (2013). Selective injection system into hippocampus CA1 via monitored theta oscillation. PLoS

Tübing, F., Vendra, G., Mikl, M., Macchi, P., Thomas, S., and Kiebler, M.A. (2010). Dendritically localized transcripts are sorted into distinct ribonucleoprotein particles that display fast directional motility along dendrites of hippocampal neurons. J. Neurosci. 30, 4160-4170.

Turrigiano, G.G., Leslie, K.R., Desai, N.S., Rutherford, L.C., and Nelson, S.B. (1998). Activity-dependent scaling of quantal amplitude in neocortical neurons. Nature 391, 892-896.

Vorhees, C.V., and Williams, M.T. (2006). Morris water maze: procedures for assessing spatial and related forms of learning and memory. Nat. Protoc. 1,

Wenk, G.L. (2004). Assessment of spatial memory using the radial arm maze and Morris water maze. Curr. Protoc. Neurosci. Chapter 8, Unit 8 5A.

Wong, R.W., Setou, M., Teng, J., Takei, Y., and Hirokawa, N. (2002). Overexpression of motor protein KIF17 enhances spatial and working memory in transgenic mice. Proc. Natl. Acad. Sci. USA 99, 14500-14505.

Wu, J.K., Tai, C.Y., Feng, K.L., Chen, S.L., Chen, C.C., and Chiang, A.S. (2017). Long-term memory requires sequential protein synthesis in three subsets of mushroom body output neurons in Drosophila. Sci. Rep. 7, 7112.

Yamazaki, H., Nakata, T., Okada, Y., and Hirokawa, N. (1996). Cloning and characterization of KAP3: a novel kinesin superfamily-associated protein of KIF3A/3B. Proc. Natl. Acad. Sci. USA 93, 8443-8448.

Yin, X., Takei, Y., Kido, M.A., and Hirokawa, N. (2011). Molecular motor KIF17 is fundamental for memory and learning via differential support of synaptic NR2A/2B levels. Neuron 70, 310-325.

Yu, G., Wang, L.G., Han, Y., and He, Q.Y. (2012). clusterProfiler: an R package for comparing biological themes among gene clusters. OMICS 16, 284-287.

Zhao, J., Fok, A.H.K., Fan, R., Kwan, P.Y., Chan, H.L., Lo, L.H., Chan, Y.S., Yung, W.H., Huang, J., Lai, C.S.W., and Lai, K.O. (2020). Specific depletion of the motor protein KIF5B leads to deficits in dendritic transport, synaptic plasticity and memory. eLife 9, e53456.





STAR***METHODS**

KEY RESOURCES TABLE

REAGENT or RESOURCE	SOURCE	IDENTIFIER
Antibodies		
Synaptophysin	Abcam	ab32594
PSD-95	Thermo Fisher Scientific	MA1-045
eGFP	Abcam	ab13970
KIF5C	Abcam	Ab5630
KIF3A	Abcam	Ab11259
Jip3	Santacruz	SC10428
GluR2	Millipore	MAB397
GluR2	Millipore	MABN71
SAP97	Epitomics Incorp.	5396-1
SLK	Bethyl Laboratories Inc.	A300-500A
β-Actin	Abcam	Ab8227
α-Tubulin	Thermo Fisher Scientific	PA1-20988
pelf2α	CST	3597
elf2α	CST	5324
MAP 2	Synaptic systems	188 004
Anti-eGFP	Fisher	NB1001614
Anti-eGFP- ChIP Grade (ab290)	Abcam	ab290
Anti-Kinesin, heavy chain	Millipore	MAB1614
Anti-Puromycin, clone 4G11	Millipore Sigma	MABE342
elF3g	Novus Biologicals	NB100-93298
CaMKIIβ-1	Thermo Fisher scientific	13-9800
SHANK2	Cell Signaling Technology	12218S
Syngap	Gift	G. Rumbaugh at Scripps Research
GluR1	Cell Signaling Technology	13185
pS6K (T389)	Cell Signaling Technology	9234
S6K	Cell Signaling Technology	9202
pS6 (S235/236)	Cell Signaling Technology	4858
S6	Cell Signaling Technology	2217
pCREB (S1233)	Cell Signaling Technology	9198
CREB	Cell Signaling Technology	9197
Bacterial and virus strains		
One Shot MAX Efficiency DH5α-T1 ^R Competent Cells	Thermo Fisher scientific	12297016
Chemicals, peptides, and recombinant proteins		
Poly-D-lysine hydrobromide mol wt. 70,000-150,000	Sigma Aldrich	P0899-100MG
Papain (PAP)	Worthington	LS003126
GIBCO DMEM, high glucose, no glutamine Cell Culture Media	Thermo Fisher	11-960-044
Neurobasal Media	Thermo Fisher	21103049
Penicillin-Streptomycin (10,000 U/mL)	Life Tech	15140-122
B-27® Supplement (50X), serum free	Thermo Fisher Scientific/Life Technologies	17504044

(Continued on next page)

Cell Reports Article



Continued		
REAGENT or RESOURCE	SOURCE	IDENTIFIER
Oulbecco's Phosphate Buffered Saline with MgCl2 and CaCl2, liquid, sterile-filtered, suitable for cell culture	Sigma	D8662-6
HyClone Dulbecco's Phosphate Buffered Saline (DPBS), 1X, without calcium, magnesium	VWR	16750-076
Fetal Bovine Serum, certified, US origin	Thermo Fisher	16000044
DMEM, high glucose, no glutamine	Thermo Fisher	11960044
HBSS (10X), calcium, magnesium, no ohenol red	Life Technologies	14065056
HEPES (1 M)	Life Technologies	15630080
Magnesium Chloride Hexahydrate	Fisher Scientific	BP214500
Sodium Pyruvate (100 mM)	Life Technologies	11360070
GlutaMAX Supplement	Thermo Fisher Scientific/Life Technologies	35050061
Glutamine	Sigma-Aldrich	G7513-100ML
UltraPure DNase/RNase-Free Distilled Water from Life Technologies	Thermo Fisher	10977023
Live Cell Imaging Solution	Life Technologies	A14291DJ
Lipofectamine 2000	Thermo Fisher	11668019
Lipofectamine® RNAiMAX Transfection Reagent	Life Technologies	13778075
Syn-PER Synaptic Protein Extraction Reagent	Fisher Sci	PI87793
4x Laemmli Sample Buffer	Bio-Rad	161-0747
SeeBlue® Plus2 Pre-Stained Standard	Thermo Fisher Scientific	LC5925
Phosphatase Inhibitor Cocktail 2	Sigma Aldrich	P5726-5ML
Phosphatase Inhibitor Cocktail 3	Sigma Aldrich	P0044
cOmplete(TM), Mini, EDTA-free Protease nhibitor Cocktail, Protease Inhibitor Cocktail Tablets	Sigma	11836170001
Superase-In. RNase inhibitor (20U/ul). 10.000 units	Thermo Fisher Scientific/Life Technologies	AM2696
Yeast RNA (10 mg/ml)	Thermo Fisher scientific	AM7118
JltraPure BSA, 250mg, 100mg/ml	MCLAB	UBSA-500
NaCl (5M)- RNase free	Thermo Fisher scientific	AM9760G
Friethanolamine, ≥ 99.0% (GC)	Sigma	90279
Acetic anhydride	Sigma	320102
Horse Serum, New Zealand origin from Life Fechnologies	Life Technologies	16050130
Goat Serum	Sigma-Aldrich	G9023-10ML
Formamide	Sigma Aldrich	F7503-250ML
nydrogen peroxide (30%)	Sigma	216763-100ML
riton (TM) X-114, laboratory grade	Sigma	X114-100ML
2-Mercaptoethanol	Bio-Rad	1610710
PKI 14-22 amide, myristoylated	Tocris, Bio-Techne	2546
Forskolin from Coleus forskohlii	Millipore Sigma	F6886
Dimethyl sulfoxide	Millipore Sigma	276855
Rolipram	Tocris	0905
Bicuculline	Sigma Aldrich	14343
Puromycin dihydrochloride from Streptomyces alboniger	Sigma Aldrich	P8833-10MG
		(0 " ,

(Continued on next page)



SOURCE	IDENTIFIER
Sigma Aldrich	C4859-1ML
Thermo Fisher	15596018
Sigma Aldrich	11685597910
Thermo Fisher	A25777
Sigma Aldrich	11685597910
•	10835269001
Biolabs	R0146S
Biolabs	R0136S
Biolabs	R0101S
Biolabs	B7204S
Quanta Biosciences - VWR	101414-106
	4309155
Sigma Aldrich	E7023
Sigma Aldrich	288306
Fisher Bioreagents	BP2618-500
Fisher Chemical	A411-4
Patterson veterinary	07-892-4348
Patterson veterinary	07-804-1040
Patterson Vet.	07-890-8115
Hanna's Pharmaceutical Supply (FISHER)	NC0628485
Hanna's Pharmaceutical Supply (FISHER)	NC0304169
VWR Intl	25608-930
Fisher Scientific	50822813
QIAGEN	28706
QIAGEN	27106
QIAGEN	28706
QIAGEN	27106
Thermo Fisher	KIT0214
Sigma Aldrich	11175025910
Thermo Fisher Scientific/Life Technologies	AM1914
Thermo Fisher	K457540
QIAGEN	12362
Perkin Elmer	NEL744001KT
Agilent	5067-1513
-	
This paper	GSE148634
• •	GSE74985
	GSE116342
51, 2310	302002
ATCC	Cot# CDI 2016 DDID:OVOL 0000
AICO	Cat# CRL-3216, RRID:CVCL_0063
	Sigma Aldrich Thermo Fisher Sigma Aldrich Thermo Fisher Sigma Aldrich Sigma-Aldrich Biolabs Biolabs Biolabs Biolabs Quanta Biosciences - VWR Thermo Fisher Sigma Aldrich Sigma Aldrich Sigma Aldrich Fisher Bioreagents Fisher Chemical Patterson veterinary Patterson veterinary Patterson veterinary Patterson Vet. Hanna's Pharmaceutical Supply (FISHER) Hanna's Pharmaceutical Supply (FISHER) VWR Intl Fisher Scientific QIAGEN QIAGEN QIAGEN QIAGEN Thermo Fisher Sigma Aldrich Thermo Fisher Scientific/Life Technologies Thermo Fisher QIAGEN QIAGEN Perkin Elmer

(Continued on next page)

Cell ReportsArticle



Continued		
REAGENT or RESOURCE	SOURCE	IDENTIFIER
Experimental models: Organisms/strains		
CD-1 E18 Pregnant female mice	Charles River Laboratories	NA
C57BL6/J mice	Jackson Laboratories, Bar Harbor, ME	NA
Oligonucleotides		
Kif3A-F	IDT	AAG CGA AAA TTG ACG AGG AG
Kif3A-R	IDT	CAT GTA AGG TTT GGT TTC CAG
Kif5C-F	IDT	CCT GAA CCT GCT TCT CAA GG
Kif5C-R	IDT	GAC CTC CGA CTT CAT CTT GC
Ubap2I-F	IDT	AGGGCTAAATCTACAGTTT GGGG
Ubap2I-R	IDT	TGAATCGGGCCACTCTG ATAA
Nova2-F	IDT	CGGCTCAATCATCGGC AAAG
Nova2-R	IDT	GCATACCCGTTCTGTAGTT CCTG
Eif3g-F	IDT	ACTACCACAGTCAGTGAT GACG
Eif3g-R	IDT	GCAGGACACAATCTTC TGGC
Syn1-F	IDT	AGCTCAACAAATCCCAGT CTCT
Syn1-R	IDT	CGGATGGTCTCAGCTT TCAC
Recombinant DNA		
peGFP-C-shLenti Kif5C	Origene	catalog# TL511686
peGFP-C-shLenti Kif3A	Origene	catalog# TL516184
scrambled shRNA	Origene	catalog# TR30013
peGFP-Kif5C-N1	Puthanveettil Lab	Puthanveettil Lab
pGL-FL <i>Kif3A</i> -C1	Addgene (Linda Wordeman)	Addgene plasmid # 13742
pRFP-C-shLenti <i>EIF3G</i>	Origene	catalog# TR30032
peGFP-C-shLenti Kif5C	Origene	catalog# TL511686
Software and algorithms		
Prism 6 (version 6.0f)	GraphPad Software	https://www.graphpad.com/ scientific-software/prism/
ImageJ	NIH	https://imagej.nih.gov/ij/
Minitab 18	Minitab Inc.	https://www.minitab.com/en-us/
Zen2.1 SP1 (Black)	Carl Zeiss	SCR_013672
MATLAB	Max Planck, Fl	GitHub - ryoheiyasuda/countSpines
Other		
ON-TARGETplus Mouse Kif5c (16574) siRNA - SMARTpool	Dharmacon	L-062091-01-0005 5 nmol
ON-TARGETplus Mouse Kif3A (16568) siRNA - SMARTpool	Dharmacon	L-042111-01-0005 5 nmol
ON-TARGETplus Non-targeting control pool siRNA	Dharmacon	D-001810-10-05 5 nmol
ON-TARGETplus Mouse Kif5c (16574) siRNA - SMARTpool	Dharmacon	L-062091-01-0005 5 nmol





RESOURCE AVAILABILITY

Lead contact

Further information and requests for resources and reagents should be directed to and will be fulfilled by the Lead Contact Sathya Puthanveettil (sputhanv@scripps.edu).

Materials availability

All unique/stable reagents generated in this study are available from the Lead Contact without restriction.

Data and code availability

RNA-Seg data can be accessed from NCBI GEO GSE148634.

EXPERIMENTAL MODEL AND SUBJECT DETAILS

For the primary cell culture preparation, pregnant CD1 mice (Charles River Laboratories) were used. For the stereotaxic injections followed by a behavioral study, 8- to 9-week-old male C57BL6/J mice (Jackson Laboratories, Bar Harbor, ME) were used. All animals were housed individually on a 12-hour light/dark cycle with ad libitum access to food and water. All experiments were performed during the light part of the diurnal cycle. Housing, animal care, and experimental procedures were consistent with the Guide for the Care and Use of Laboratory Animals and approved by the Institutional Animal Care and Use Committee of Scripps Research, Florida.

HEK293 cell culture

HEK293 cells were grown in DMEM (GIBCO 11-960-044) with 10% fetal bovine serum (FBS), 1% penicillin-streptomycin, and 5 mM glutamine. In brief, cells were seeded in T75 flask and sub-cultured for the preparation of lentivirus vectors.

METHODS DETAILS

Neuronal cell cultures

Primary HP neuron cultures were prepared from the brains of embryonic day 17-18 mice as described previously (Banker and Goslin, 1988). Briefly, hippocampi were removed from embryonic day 18 mouse brains and dissociated with papain (29.5 U/mg protein, Worthington). Cells were plated at a density of 5×10^5 on poly-D-lysine-coated (100 μ g/ml, Sigma in RNase-free water) dishes and 1 \times 10⁵ glass coverslips. Cultures were plated in Neurobasal medium supplemented with 10% fetal bovine serum and penicillin/streptomycin mix and grown in Neurobasal medium supplemented with 2% B27, 0.5 mM glutamine, and penicillin/streptomycin mix at 37°C in 5% CO_2 .

Constructs and transfection

pEGFP-C-shLenti against KIF5C (catalog# TL511686), pEGFP-C-shLenti against KIF3A (catalog# TL516184) and a scrambled shRNA control (catalog# TR30013) were obtained from ORIGENE. pEGFP-KIF5C-N1 was prepared at Puthanveettil Lab and pGL-FLKIF3A was a gift from Linda Wordeman (Addgene plasmid # 13742). DNA constructs for transfection were purified using an Endo-Free Plasmid Maxi kit. siRNAs/shRNAs were introduced to primary HP neurons (DIV 14) using Lipofectamine RNAiMAX or Lipofectamine 2000 according to the manufacturer's guidelines. One day before transfection, the fresh culture medium was prepared and mixed evenly with the old medium. One-half of the mixed medium was left with the cells for transfection, and the other half was saved for medium replacement after transfection. Briefly, for the shRNA transfection to KD KIF5C and KIF3A of cells growing in the single well of a 24-well format dish, 0.2 μg DNA was mixed with 1.25 μL of Lipofectamine 2000 in 100 μL of DMEM and incubated for 25 min. The complexes of DNA and Lipofectamine 2000 were added to the cells for 2 hours incubation at 37°C in 5% CO₂. Cells were then returned to the saved culture medium. A similar strategy was followed for the OE of both KIF5C and KIF3A in primary HP neuron cultures.

Measurements of mEPSCs

Coverslips with cultured HP neurons (DIV 16-18) were transferred to the perfusion chamber of an upright microscope and perfused with extracellular bath solution (EBS) containing (in mM): 135 NaCl, 10 glucose, 3 CaCl₂, 2 KCl, 2 MgCl₂, and 5 HEPES, pH adjusted to 7.3-7.4 with NaOH, and 300-315 mOsm with sucrose. Recordings were performed to measure mEPSCs under voltage clamp. Wholecell patch-clamp recordings were performed using an Axon Multiclamp 700 b amplifier, 1440A Digidata digitizer and pClamp software (Axon Instruments, Foster City, CA). Recordings were made at 50 kHz and subsequently filtered at 5 kHz. The recordings were conducted blindly during these experiments; HP neurons were cultured for at least 16 days to allow an extensive synaptic network to develop before recordings were made. The mEPSCs were recorded in the presence of TTX at 1 µM. The membrane potential was held at -60 mV during the recording of sEPSCs as well as during the recording of mEPSCs. The current-clamp recording was taken only to identify the health of the neurons. Only neurons with a resting membrane potential of less than -40 mV were used for our

Cell Reports Article



analysis. Action potentials were recorded in current-clamp mode, I = 0. The membrane potential was maintained at -40 mV in current-clamp mode. All experiments were performed at room temperature (22-24°C). The frequency and amplitude of EPSCs were analyzed using the template match search (pClamp), and basic statistical analysis was performed to extract the average amplitude and frequency. The amplitude and frequency of EPSCs expressed as a percentage of baseline level, calculated from an average of 5 min of the baseline-recording period. The amplitude and frequency of EPSCs for each experiment were measured as an average of 5 min during the recording period. Each of the n-values shown refers to the number of neurons recorded. The term significant denotes a relationship with p < 0.05 determined using an unpaired, two-tailed Student's t test and one-way ANOVA followed by a post hoc test. For the analysis of the cumulative probability of the amplitude and the cumulative probability of inter-event intervals, a two-sample Kolmogorov-Smirnov (KS test) was taken into the analysis, and the difference was considered significant when p < 0.05.

Live imaging

Seventy-two hours after transfection, live eGFP-tagged neurons were observed and images were captured at the light microscopy facility, the Max Planck Florida Institute, using a confocal microscope (LSM 780; Carl Zeiss; Plan Neofluor 63X/1.3 N.A. Korr differential interference contrast M27 objective in water) at room temperature. Z stack images were acquired using ZEN 2015 (64 bit) software (Carl Zeiss), and dendritic arbors were manually traced and later quantified by Sholl analysis FIJI (ImageJ, NIH). A series of concentric circles were drawn from the center of the soma at intervals of 20 µm, with the radius of the outermost circle set at 100 µm. The maximum value of sampled intersections reflecting the highest number of processes/branches in the arbor was calculated, and the number of intersections plotted against distance from the soma center in μm. To analyze spines, images captured at 63X objective and secondary branches from basal and apical dendrites were selected as the region of interest from the original image stack using MATLAB software developed in the light microscopy facility at the Max Planck Florida Institute (GitHub - ryoheiyasuda/ countSpines). By using a geometric approach, this software automatically detects and quantifies the structure of dendritic spines from the selected secondary branch (100 µm length) in the Z stack confocal image. The software assigns the detected spines to one of the three morphological categories (thin, stubby or mushroom) based on the difference in structural components of the spines i.e., head, neck and shaft. Unpaired, two-tailed Student's t test or one-way ANOVA followed by a post hoc test was carried out to evaluate significant differences among the groups.

Characterization of KIF5C and KIF3A overexpression (OE) plasmids

KIF5C could function as homo-dimers or heterodimers with KIF5A or KIF5B whereas KIF3A function requires association with KIF3B and KAP3 (Yamazaki et al., 1996; Hirokawa et al., 2009). We assumed that overexpression of KIF5C could result in enhanced levels of KIF5C homodimers and also recruit KIF5A and KIF5B from the cytoplasm. Similarly, overexpression of KIF3A could make functional complexes by recruiting KIF3B and KAP3. Therefore, we first assessed whether the full-length (FL) KIF-eGFP fusion proteins are functional in neurons by performing fluorescence recovery after photobleaching (FRAP) measurements. Unlike the appearance as discrete puncta along dendrites that we observed in super resolution imaging of native KIF5C and KIF3A (Liu et al., 2014), the overexpression of KIF5C and KIF3A as fusion proteins resulted in diffused green signals throughout the neuron. Functional Kif fusion proteins are expected to show a faster recovery time after bleaching than eGFP as the result of active directional transport.

Therefore, we performed FRAP measurements (N = 11, 16 and 9 for eGFP, KIF5C FL and KIF3A FL, respectively). HP neurons were transfected using Lipofectamine 2000 at DIV 14 and used for a FRAP assay 24 hours after transfection. Neurons expressing eGFP, KIF3A FL or KIF5C FL were analyzed at the light microscopy facility, the Max Planck Florida Institute, using a confocal microscope (LSM 780; Carl Zeiss; Plan Neofluor 63X/1.3 N.A. Korr differential interference contrast M27 objective in water) at room temperature. Regions of interest (ROIs) of the same size were photobleached by scanning with a 405 nm and 488 nm laser combined at the maximum power. Images were first acquired for 156 s at a time interval of 0.781 s at low intensity to establish baseline intensity values, bleached over an approximately 10-micron region of the axon at high power for 78 s and recovery was monitored using low power for 156 s. Movies were uploaded to ImageJ, and stage drift was corrected in some movies using the ShearX plugin in both the x and y directions. A 1 μm wide region (i.e., 20 pixels with magnification at 0.0527 μm/pixel) was selected along the middle of the process using the freehand line tool and straightened using the straightened function in ImageJ. The straightened images were cropped to select only the bleached region. The sum of the pixel intensity as a function of time over the cropped region was then measured for each group. In order to calculate the half-life of recovery, the average pixel intensity over the prebleach time was first measured; next, the intensity during the recovery phase was transformed into linear coordinates using the equation I_{transformed}(t) = $ln(1-l_{observed}(t)/l_{prebleach})$. Linear regression was used to measure the recovery constant $k_{recovery}$ over the first 15.6 s for each neuron, which was converted into recovery half-life with the equation $t_{1/2} = -0.693/k_{recovery}$. Data are presented as the mean \pm SEM analyzed by one-way ANOVA followed by a post hoc Fisher's LSD test.

Based on the average intensities over the first and last 8 s in the prebleach condition, the bleaching at the low intensity was less than 5%. The data were exported to Minitab and analyzed using one-way ANOVA and a post hoc Fisher's least significant difference (LSD) test (p = 0.031; Figures S1G-S1I; Table S1). The half-life of eGFP (105.2 \pm 26.8) was double that of KIF5C OE (50.8 \pm 5.9) or KIF3A OE (57.2 ± 6.3), indicating that both KIF5C and KIF3A fusion proteins are functional. Taken together FRAP assay suggest that overexpression of KIF5C and KIF3A produce functional transport machineries in hippocampal neurons.

As an independent measure of the function of KIF fusion proteins, we examined the distribution of KIF5C and KIF3A protein cargos in OE neurons. We reasoned that functional OE would result in enhanced dendritic localization of specific cargos. In our previous





work (Liu et al., 2014), we identified specific cargo molecules for KIF5C (Jip3 and GluR2) and KIF3A (SAP97 and SLK). We first assessed the expression levels of KIF5C and KIF3A in OE neurons. We found a significant increase in the mean fluorescence intensity in *KIF5C*-overexpressing (161.6 \pm 13.0) neurons compared to control neurons (100 \pm 5.8; N = 3, p = 0.012) and in *KIF3A*-overexpressing (191.2 \pm 18.09) neurons compared to control neurons (100 \pm 21.1; N = 4, p = 0.017; unpaired, two-tailed Student's t test; Figures S1J–S1M; Table S1). Next, we examined the distribution of their protein cargos in dendrites of OE neurons by immunostaining using specific antibodies. Our results indicate that there was a two-fold increase in the mean fluorescence intensity of Jip3 in dendrites of *KIF5C*-overexpressing (14.2 \pm 1.75) neurons compared to the control (8 \pm 0.9; N = 6, p = 0.012). Additionally, there was a four-fold increase in the mean fluorescence intensity of GluR2 in *KIF5C*-overexpressing (4 \pm 0.9) neuronal dendrites compared to the control (1 \pm 0.2; N = 6, p = 0.008). We found that the mean fluorescence intensity of SAP97 was nearly doubled in dendrites of *KIF3A*-overexpressing (12.14 \pm 1.9) neurons compared to control neurons (5.3 \pm 0.7; N = 7, p = 0.0057), and the same was true of the mean fluorescence intensity of SLK staining (*KIF3A* OE: 50.2 \pm 6.2; eGFP control: 20.4 \pm 3.5; N = 6, p = 0.0019; unpaired, two-tailed Student's t test; Figures S1A–S1F; Table S1).

To further characterize KIF5C OE, we imaged pre- and postsynaptic protein markers in KIF5C OE neurons. We carried out PSD-95 and synaptophysin immunocytochemistry (ICC) in eGFP-expressing primary neurons. PSD-95 is a postsynaptic marker (Rao et al., 1998), whereas synaptophysin is a presynaptic vesicle membrane protein (Fykse et al., 1993; Marquèze-Pouey et al., 1991). Using fluorescence intensity measurements, we found a two-fold increase in PSD-95 expression in neurites of cells overexpressing KIF5C (19.9 \pm 3.3) compared to control eGFP (10.2 \pm 1.8; N = 5, p = 0.04; unpaired, two-tailed Student's t test; Figures S1N and S1O; Table S1). However, synaptophysin expression was comparable between neurites of KIF5C-overexpressing and control cells. These data further support that the changes in mEPSCs in OE neurons are mediated through a postsynaptic mechanism (Figures S1N and S1P; Table S1).

Overexpression of KIF5C and knockdown of KIF3A in the same neurons

Our results showing that *KIF5C* and *KIF3A* KDs produced deficits in synaptic transmission and neuronal architecture, whereas only *KIF5C* OE produced an enhancement in them, led us to ask whether *KIF5C* OE might recruit *KIF3A* for enhancing synapse density and dendritic arborization. To address this, we performed *KIF3A* KD in *KIF5C* OE HP neurons and quantified changes in spine morphology and dendritic arborization. If *KIF5C* OE recruit *KIF3A* for its morphology enhancing effects, we expect to observe a blockade of *KIF5C* OE effects with *KIF3A* KD on neuronal morphology.

We used the eGFP-tagged KIF5C OE plasmid described above and prepared an RFP-tagged KIF3A KD plasmid for neuronal transfections. eGFP alone and RFP alone expressing neurons were used for comparisons in the confocal live-cell imaging. We found that KIF5C OE resulted in increased spine density despite KIF3A KD in the same neurons (N = 25; unpaired, two-tailed Student's t test, p < 0.0001; Figure 2O; Table S1). We observed a significant increase in the number of mushroom spines in KIF5C OE + KIF3A KD neurons compared to control (p = 0.046; unpaired, two-tailed Student's t test) and a significant decrease in thin spines in KIF5C OE + KIF3A KD compared to control (p = 0.0065; unpaired, two-tailed Student's t test) neurons. No significant change was observed in stubby spine morphology in KIF5C OE + KIF3A KD neurons compared to the control (p = 0.14 unpaired, two-tailed Student's t test; Figure 2P; Table S1).

Next, we assessed dendritic arborization in *KIF5C* OE + *KIF3A* KD neurons by Sholl analysis. Consistent with the spine density and morphology data, we found significant increases in dendritic branching in *KIF5C* OE + *KIF3A* KD neurons compared to controls at multiple distances from the soma: 30-60 μ m whereas, there were no significant differences at 20 or > 70 μ m from soma (p < 0.01; unpaired, two-tailed Student's t test; Figures 2Q and 2R; Table S1). Collectively, these results indicate that the effects of *KIF5C* OE on spine morphology and dendritic arborization are independent of *KIF3A* expression in the same HP neurons.

Immunocytochemistry (ICC) and fluorescence in situ hybridization (FISH) analysis

Primary cultured HP neurons on glass coverslips were processed for ICC 24 or 72 hours after transfection. Neuronal culture medium was carefully removed, and after two rinses in PBS, the cells were fixed in a freshly prepared solution of 4% paraformaldehyde for 15 min. After two more rinses in PBS, the cells were permeabilized in 0.5% Triton X-100 in PBS for 15 min. The cells were then incubated in 8% normal goat serum (Sigma) in PBS for 45 min and incubated with primary antibody (Refer key resources table for Antibody details) at 4°C overnight. The immunoreactivity was probed using 405-, 488- or 568-conjugated secondary antibodies (1:500; Molecular Probes) for 1 hour at room temperature. For mounting, fluoro gel II (17985-10, Electron Microscopy Sciences) without DAPI was used. The images were taken with a Zeiss LSM780 confocal microscope. For assessing the dendritic localization of KIF5C associated RNAs SYN1 and EIF3G, briefly a 200 bp fragment from SYN1 or EIF3G cDNAs were cloned into a dual TOPO II vector for making Digoxigenin (DIG) labeled riboprobes. FISH experiments using DIG labeled riboprobes were carried out as described in Liu et al., 2014 and Raveendra et al., 2018. Localization of SYN1 and EIF3G were visualized by SIM imaging described below.

KIF5C coimmunoprecipitation (CoIP), RNA-Seq and bioinformatics analysis

Following previously published methodology for KIF5C complex CoIP from the hippocampus (Liu et al., 2014), we isolated RNAs from the precipitates. Briefly, Iysates were prepared using Iysis buffer: 0.50% Nonidet P-40, 50 mM Tris-HCl pH 7.5, 125 mM NaCl, 1 mM EDTA pH 8.0, 1 mM DTT, 1 protease inhibitor cocktail tablet (Roche), 100 μL of phosphatase inhibitor cocktail 1 and 2 each (Sigma), and 100 μL BSA. Following Iysis for 30 min at 4°C, Iysates were centrifuged to remove any debris and subjected to CoIP using a

Article



previously characterized kinesin antibody (MAB6414, Millipore; Liu et al., 2014). Mouse IgG antibody (IgG control Ab 08-6599 Thermo Fisher) was used as a control. For each Co-IP, we used hippocampi from two adult C57BL/6 mice (7-9 weeks old). For the RNA-Seq analysis, we pooled 6 different Co-IP samples into two samples (12 animals for KIF5C Co-IP and 12 animals for Control Co-IP; N = 2 for each condition for RNA-Seq). Following IP, RNAs were isolated using the TRIzol method and submitted to Scripps Genomics Core for Processing. RNA libraries were prepared for sequencing using standard Illumina protocols (Raveendra et al., 2018). All samples were processed and sequenced on a NextSeq 500. The quality of the reads overall was quite high, with no decrease in quality over the course of sequencing. After quality control, the reads were mapped to the mouse transcriptome using Salmon using paired-end settings (Salmon reference was made using Ensembl: ftp://ftp.ensembl.org/pub/release-99/fasta/mus_musculus/cdna/Mus_ musculus.GRCm38.cdna.abinitio.fa.gz). Ensembl transcript IDs, raw counts, and TPM values were imported into R (Yu et al., 2012). Differential expression analysis between the KIF5C IP and IgG IP transcripts was performed using DEseq2 (n = 2 per group), and padjusted < 0.05 was used as a cutoff for assessing dendritically targeted transcripts, yielding 2906 transcript isoforms from 2399 genes. RNA-Seq data can be accessed from NCBI GEO GSE148634 (https://www.ncbi.nlm.nih.gov/geo/query/acc.cgi?acc= GSE148634). Gene Ontology analysis was performed in R using the Cluster Profiler Bioconductor package with an adjusted p value cutoff such that FDR < 0.05. Reactome pathway analysis was performed using the Reactome PA package with a p value cutoff of 0.05.

Next we compared KIF5C-associated RNAs with mouse hippocampal transcriptome (Cembrowski et al., 2016) and mouse neuropil transcriptome (Farris et al., 2019) and rat neuropil transcriptome (Cajigas et al., 2012). The overlapping genes were analyzed as follows: RNaseq data for; Farris et al., 2019., were independently analyzed from GEO-obtained fastq files using the methods described above. Briefly we downloaded GSE74985 (single end reads: Cembrowski et al., 2016) and GSE116342 (paired end reads: Farris et al., 2019) and then mapped to mouse transcriptome using Salmon. GSE74985 data consists of 3 biological replicates each of dorsal and ventral CA1, CA2, CA3 and DG. We summed up all the reads for the dorsal and ventral hippocampal regions to get total hippocampal reads for the 3 biological replicates. We calculated the average TPM of the 3 replicates and used an average TPM cutoff of > 2, resulting in 21499 genes used for the venn diagram. GSE116342 data consists of 3 biological replicates each of cell body and dendritic layers of CA1, CA2, CA3 and DG (24 samples total). For each biological replicate, the reads were summed up for the sub regions in dendrites and separately for cell body to get total hippocampal dendritic and cell body reads (6 groups total: N = 3 dendrite and N = 3 cell body). We next ran DEseg2 on Dendrite versus Cell Body (N = 3 per group) and took padj < 0.05, log2FoldChange > 0 (dendrite enriched RNAs), and average TPM > 2 (Consistent with Cembrowski paper cutoff) resulting in 5007 genes used for the venn diagram. Data from Cajigas et al., was obtained from Table S3 (filtered neuropil list). Venn diagram was plotted using BioVenn (Hulsen et al., 2008). Also see Tables S2, S3, and S4.

Structured illumination super-resolution microscopy (SIM)

Following FISH or ICC, neurons were imaged using a Zeiss ELYRA PS.1 instrument (Carl Zeiss, Jena, Germany) at a resolution of 1028 by 1028 pixels, using a Zeiss 63x/1.4 NA Plan Apochromatic objective. Each fluorescent channel, 405, 488 and 561, was acquired using three pattern rotations with 3 translational shifts. The final SIM projection images were reconstructed using Zen 2013 (Carl Zeiss, Jena, Germany) and analyzed using ImageJ.

Characterization of synaptoneurosomes

Based on previous studies, a decrease in the ratio of elf2 α phosphorylation (peif2a) to total elf2 α is indicative of an increase in protein synthesis (Costa-Mattioli et al., 2005). We found a significant decrease in the peif2a/eif2a ratio in forskolin-exposed neurons (60 ± 12.0) compared to the control (100 ± 9.8) (N = 5; unpaired, two-tailed Student's t test, p = 0.0361, Figures S3A-S3C; Table S1), suggesting an increase in protein synthesis. Thus, we considered the peif2a/eif2a ratio in synaptoneurosomes to be a reliable measure of translational activation at the synapse. We first verified the quality of synaptoneurosome preparation from HP neurons by western blot (WB) analyses of fractions such as homogenate, cytosol, and synaptoneurosomes for enrichment of key synaptic proteins. We found more than 7-fold enrichment of PSD-95 and synaptophysin protein levels in the synaptoneurosome fraction compared to the homogenate and cytosol fraction in HP neurons (Figures S3D-S3F; Table S1).

Optimization of puromycin labeling of newly synthesized proteins

To establish puromycin labeling of newly synthesized proteins, we asked whether newly synthesized proteins due to forskolin exposure could be detected by puromycin labeling. WB analysis of synaptoneurosomes (Figure S3H) showed that forskolin produces an increase in puromycin-labeled proteins, suggesting an enhancement in local translation in forskolin-treated neurons (166.6 ± 18.05) compared to the control (100 ± 11.4, N = 3, *p < 0.01; unpaired, two-tailed Student's t test; Figures S3G–S3I; Table S1). In addition, we carried out immunostaining in primary neurons and found that consistent with our WB data, forskolin produced increased staining of puromycin-labeled proteins in soma when compared to the control (N = 6, *p = 0.0447; unpaired, two-tailed Student's t test; Figures S3J and S3K; Table S1).

Puro-proximity ligation assay (PLA)

PLA was performed as previously described (tom Dieck et al., 2015). Primary hippocampal neurons were treated with Puromycin (3 uM) for 10 minutes, washed with warm PBS and fixed in 4% PFA/4% Sucrose for 15 minutes. After 2 more rounds of PBS washing,





and blocking in 5% horse serum in 0.1% Triton X-100 PBS, neurons were then incubated with mouse anti-puromyin antibody (1:2000, Sigma, MABE342) and one of rabbit antibody for C terminus elF3g (1:1000, Novus Biologicals, NB100-93298), GluR1 (1:1000, CST, 13185), or CamKIIβ-1 (1:1000, Sigma, 13-9800) overnight. PLA was then performed using Duolink Reagents (Sigma, 92008) as per instructions. Cells were mounted using Duolink in situ mounting medium and imaged using Structured Illumination Microscopy.

Synaptic protein extraction and western blotting

Primary cultured HP neurons on 6-well plates were processed for synaptoneurosome preparation followed by 30 min of forskolin (50 μm) treatment. Neuronal culture medium was carefully removed, and after two rinses in ice-cold PBS, cells were lysed manually in Syn-Per buffer (Syn-PERTM Synaptic Protein Extraction Reagent) supplemented with 1 protease inhibitor cocktail tablet and 100 μL of phosphatase inhibitor cocktail 1 and 2 each. Samples were centrifuged at 1200 \times g for 10 min at 4°C, the pellet was discarded, and the supernatant was transferred to a new tube. Twenty-five microliters from the sample of the supernatant was saved as homogenate for analysis. The supernatant was centrifuged at 15,000 × g for 20 min at 4°C. The supernatant was removed from the synaptosome pellet and saved as the cytosolic fraction for analysis. The synaptosome pellet was suspended in 30 μL Syn-PER. For the WB analysis, the protein concentration was determined using a BCA kit. Protein (10-25 μg) was used for WB analysis. The antibodies used are listed in the key resources table. The target proteins were detected using anti-rabbit or anti-mouse secondary antibodies at a 1:5000 dilution and then visualized by chemiluminescence (Amersham Biosciences, Piscataway, NJ). The autoradiograms were analyzed by ImageJ.

Synaptic protein extraction and immunoprecipitation

Primary cultured HP neurons on 6-well plates were infected with Lenti eGFP-L10 virus (8 × 10⁷ TU/ml) at DIV 4, and DIV 14 expression of KIF5C was KD. Cells were processed at DIV 17 for synaptoneurosome preparation followed by 30 min of forskolin (50 μm) treatment. Neuronal culture medium was carefully removed, and after two rinses in ice-cold PBS, cells were lysed manually in Syn-Per buffer and processed as mentioned above. Synaptosome pellets were suspended in 50 µL IP buffer Nonidet P-40 lysis buffer (0.25% Nonidet P-40, 50 mM Tris-HCl pH 7.5, 150 mM NaCl, 1 mM EDTA pH 8.0, 1 mM DTT, 1 protease inhibitor cocktail tablet, 100 μL of phosphatase inhibitor cocktail 1 and 2 each, 100 μL BSA, 200 μL Yeast t-RNA, 40 U SUPERase In RNase Inhibitor) and kept on a rotator for 15 min at 4°C using a refrigerated centrifuge. For immunoprecipitation of L10, KIF5C KD synaptoneurosomes were incubated with 2 µL of eGFP antibody, and all the incubations were kept on a rotator overnight at 4°C. Then, we added 40 μL of a 50% (w/v) slurry of protein A/G beads and incubated for 1 hour at 4°C. IPs were then briefly centrifuged (100 \times g for 2 min), and the slurry was washed three times with wash buffer (0.25% Nonidet P-40, 50 mM Tris-HCl pH 7.5, 150 mM NaCl, 1 mM EDTA pH 8.0, 1 mM DTT, 1 protease inhibitor cocktail tablet, 100 µL of phosphatase inhibitor cocktail 1 and 2 each). The resulting precipitated protein complexes were used for RNA isolation.

RNA isolation, reverse transcription and qRT-PCR

After lentivirus EGFP and L10A-EGFP transduction or knockdown of KIF5C for 72 hours using siRNA, DIV 17 cultured primary neurons were briefly washed with RNase-free PBS, and cells were lysed to isolate RNA according to the manufacturer's protocol using the Ambion® RNAqueous®-Micro Kit (AM1931, Life Technologies Corp.) or Arcturus Pico Pure Isolation Kit (12204-01, Applied Biosystems, Life Tech.). The purified RNA was quantified using Qubit Fluorometer 2.0 (Q32866, Invitrogen), and quality was assessed using an Agilent RNA 6000 Pico Kit (5067-1513, Agilent Technologies, Santa Clara, CA). Total RNA (1 µg of each sample) was reverse transcribed to cDNA using qScriptTM cDNA SuperMix (95048-100, Quanta BiosciencesTM). The concentration and purity of the resultant cDNA were determined using a Nanodrop spectrophotometer (NanoDrop, Wilmington, DE).

The expression of genes was quantified by quantitative real time PCR (qRT-PCR or qPCR) using SYBR Green PCR master mix (Applied Biosystems Carlsbad, CA) as described previously (Liu et al., 2014; Kadakkuzha et al., 2015). All of the qPCR amplifications were performed in a total volume of 10 μL containing 2 μL of H₂O, 2 μL of cDNA, 5 μL of the 2X Master mix, and 1 μL of 10 μm (each) forward and reverse primers (key resources table). All the genes were tested for the expression of mouse 18S rRNA, and the 1/2Ct *value was calculated. Quantification of each transcript was normalized to the mouse 18S reference gene following the $2-\Delta\Delta$ Ct method (Livak and Schmittgen, 2001). Unpaired, two-tailed Student's t test was used to select genes with statistically significant expression levels where *p value < 0.05. (For the sequences of the primers used in this study, refer to key resources table).

Chemical long-term potentiation (cLTP)

8-9 weeks old C57BL6 male mice were sacrificed by cervical dislocation, brain isolated and kept in normal artificial CSF (NaCl 125mM, KCl 2.5mM, $MgCl_2 + 6H_2O 1mM$, $CaCl_2 + 2H_2O 2mM$, $NaH_2PO_4 + H_2O 1.25 m$, $NaHCO_3 26mM$, D-Glucose 11mM; pH = 7.3) and oxygenated at (95% O₂/ 5%CO₂) (Ch'ng et al., 2012). Acute hippocampal coronal slices were obtained using a vibratome (Leica) at 300 µm. Post sectioning, slices were incubated in a chamber at 32°C with regular artificial CSF and 95% O₂/5% CO₂ for stabilization before the stimulation. For cLTP, slices were transferred to a new ACSF solution without MgCl₂ that includes Forskolin (50μM), Rolipram (100nM) and Bicuculline (40µM) and incubated for 15min or 1hour. Immediately after stimulation of the cLTP, CA1 hippocampal area was dissected and lysed in 200ul of Syn-Per reagent with protease and phosphatase inhibitors. Then, samples were centrifuged at 4000xg for 10min at 4°C to collect the supernatant. Immunoblotting was carried out as mentioned in previous section to detect KIF5C and GluR2 expression.



Preparation of lentiviral vectors

pEGFP-C-shLenti against KIF5C (catalog# TL511686C) and scrambled shRNA control (catalog# TR30013) were obtained from ORI-GENE. pEGFP-KIF5C-FL was cloned into the lenti backbone by the Molecular Biology Core at Max Planck Florida Institute, and control eGFP lentivirus (CV10002) was purchased from Vigene Biosciences. Each plasmid was cotransfected with HIV-1 packaging vector p8.91 and the Vesicular stomatitis virus (VSV) G-protein into human embryonic kidney (HEK) 293 cells to produce viral particles using Mirus reagent. The supernatant was collected 48-72 hours later. Viral particles were concentrated and pelleted through the sucrose cushion. The viral pellet was then resuspended in sterile PBS and stored at -80°C. Viral titer was determined by measuring GFP fluorescence after infection of HEK293 cells with serial dilutions of the virus using flow cytometry (BD Biosciences C6 Accuri and IntelliCyt HyperCyt sampler powered by FlowCyt software). For KIF5C KD lenti virus preparation we used mouse, unique 29-mer shRNA constructs in lentiviral GFP vector backbone and for respective control we used non-effective 29-mer scrambled shRNA cassette in pEGFP-C-shLenti Vector. For KIF5C OE the eGFP fusion proteins (C terminus) under the control of the CMV promoter backbone and for respective control virus eGFP with the vector backbone pEGFP-C-shLenti were used. The viral titer of KIF5C KD and scrambled shRNA control lentivirus was 1×10^9 TU/ml and for KIF5C OE and control EGFP was 1 × 10¹⁰ TU/ml used for stereotaxic injections and downstream experiments.

Characterization of lentiviral vectors

We prepared lentiviral vectors for KIF5C KD based on the shRNA data we described in Figure 1 and delivered by stereotaxic injections into the dorsal CA1. We first examined the expression levels of KIF5C in CA1 following its KD by lentivirus-mediated expression of shRNA construct in CA1. Western analysis of brain punches from hippocampal CA1 regions showed a significant decrease in the protein expression in KIF5C KD lentivirus injected mice (82.23 ± 3.23) as compared to control virus injected mice (100 ± 5.08; N = 8, p = 0.0105; unpaired, two-tailed Student's t test; Figures S6B and S6C; Table S1).

Similarly, we assessed the expression levels of KIF5C OE in lentivirus-injected mice by immunoblotting. We found a significant increase in the protein expression in brain punches obtained from CA1 region of KIF5C OE lentivirus injected mice (148.26 \pm 19.56, N = 18) when compared to control virus injected mice (100 ± 6.51; N = 15, p = 0.0173; unpaired, two-tailed Student's t test; Figures S6D and S6E; Table S1)

Stereotaxic injections

For the surgeries, we used only male mice on a pure C57BL/6 genetic background to avoid variability derived from the estrus cycle during the behavioral experiments (Cover et al., 2014; Lebrón-Milad et al., 2013). Stereotaxic surgical procedures were performed under anesthesia (1.0%-1.5% isoflurane), and animals were mounted on stereotaxic frame instruments (Kopf Instruments, Tujunga, CA, USA). An incision was made along the midline of the scalp, and the skull was exposed. Small burr holes were drilled into the skull at the following coordinates (2.18 mm posterior to bregma, ± 1.6 mm lateral to the midline, 2.5 mm deep with respect to the skull surface (Franklin and Paxinos, 1996; Tsutajima et al., 2013)). Lentiviral particles were injected bilaterally using a 10 μL Hamilton syringe (model 33BV needle) at a volume of 1 μL per site (flow rate of 50 nl/min). Metacam was administered preoperatively at a dose of 5 mg/kg as injectable solution subcutaneously in the scruff, and Baytril was administered postoperatively at a dose of 10 mg/kg as injectable solution intramuscularly using a 1 cc syringe and a 25 or 27 Ga needle. After surgery, animals were housed individually and given at least 5 days of recovery during which they were monitored daily to check their health condition. Proper postoperative care was performed to ensure that animals experienced little or no discomfort, and animals showing signs of pain and/or obvious discomfort outside this time were removed from the study and euthanized.

Behavioral tests

All behavioral tests were performed in an individual, dedicated experimental room. Lentivirus-injected animals undergo handling three days before the behavior task for acclimation to transport from their home cages to the holding room. On the testing day, animals were put in the test room at least 30 min before testing to acclimatize. The experimenter was always blind to the treatment type when performing the tests.

Morris water maze (MWM)

The MWM task was performed as previously described (Vorhees and Williams, 2006; Wenk, 2004). Briefly, MWM testing was conducted in a round white pool 120 cm in diameter, located in a room with visible external cues. The pool was filled to a depth of 30 cm with water made opaque with white nontoxic water-based white paint. The pool temperature was maintained at 22 ± 0.5°C by the addition of warm water. The escape platform was a 10 cm plexiglass circle placed in the center of one quadrant of the pool, 20 cm from the pool's edge and submerged 1.5 cm beneath the water surface. The platform and visual cue remained in the same position throughout the learning trial tests and were removed from the pool during the probe test. During the acquisition trials (days 1 to 6), mice were trained to escape from water by swimming from variable starting points around the tank to a hidden platform (10 cm diameter) and allowed to remain there for 10 s. Each training day consisted of 4 different trials separated by 15-20 min. The maximum swim time was set to 60 s. If the mouse located the platform before 60 s had passed, it was immediately removed from the pool.

If the platform was not located after 60 s of swimming, the mouse was guided to the platform and/or placed on it for 10 s. After each trial, mice were dried and returned to their home cages. After removal from the pool, mice were manually dried with a sterilized paper towel and placed in the home cage placed in the warming chamber (consisting of a heating pad set to low underneath cage) for at





least 5 min before returning to the holding room. Mice were visually inspected to ensure thorough dryness. Twenty-four hours after finishing the training, the platform was removed from the tank, and the mice were allowed to swim for 60 s in a single trial. Spatial learning was measured by latency to the platform, distance, and velocity. The LTM test consists of time spent in Q1, the number of platform crossings and the number of visits to Q1, as well as its comparison with Q4. All testing was conducted at roughly the same time each day to minimize variability in performance due to the time of day. All sessions were recorded by a digital tracking system connected to a video camera (Panasonic, WV-BP334, Osaka, Japan) located above the tank and different parameters measured by EthoVision XT software. The resultant behavioral data were statistically analyzed.

Contextual fear conditioning (CFC)

CFC was performed as previously described (Rizzo et al., 2017). Briefly, experiments were performed using a set of four modified Noldus PhenoTyper (Model 3000) chambers (Leesburg, VA) with shock floors (Burgos-Robles et al., 2009). The PhenoTyper Model 3000 chamber has a 30 $\text{Å}\sim$ 30 cm floor and is 40 cm in height. The PhenoTyper chamber is equipped with a top unit, including a matrix of infrared LED lights and an infrared CCD camera, with a high-pass filter blocking visible light. The floor of the cages included a stainlesssteel grid (bar spacing: 0.9 cm) connected to an electric shock generator (Shock Scrambler ENV-414S; Med Associates, St. Alvans, VT). Automated tracking and shock delivery control were performed using EthoVision 8.5 software (EthoVision 8.5; Noldus Information Technology, Leesburg, VA; https://www.noldus.com/ethovision). Each chamber was cleaned with 70% ethanol before each trial. White light was used inside the chamber for training and testing, and 72 db white noise was played in the room to mask any unintended noise that might add to the context. During the fear conditioning session, mice received three 2 s, 0.75 mA scrambled foot shocks 2.5, 3.5, and 4.5 min after placement into the chamber. Mice were promptly removed from the chamber after 5.5 min. Twenty-four hours later, mice were tested for CFC by placing them back into the chambers for 5 min. The percentage of time spent freezing (immobility except for breathing) was recorded in both training and testing sessions using EthoVision XT 11 (Noldus Information Technology, Inc).

Low shock CFC and extinction experiment was performed in KIF5C OE and control mice as previously described (Ortiz et al., 2010) using our similar experimental set-up as discussed above with slight modification. During the fear conditioning session, mice received three 2 s, 0.4 mA scrambled foot shocks 2.5, 3.5, and 4.5 min after placement into the chamber. Mice were promptly removed from the chamber after 5.5 min. Twenty-four hours later, mice were tested for CFC by placing them back into the chambers for 30 min. The first 5 min recording for twenty-four-hour test and % freezing extinction recorder every 5 min for 30 min After 24 hr extinction to assess the long-term memory recall test is performed for 5 min for every min bin. The percentage of time spent freezing (immobility except for breathing) was recorded in both training and testing sessions using EthoVision XT 11 (Noldus Information Technology, Inc).

Histological analysis

Brains were collected after completion of behavioral testing and post fixed in 4% paraformaldehyde (PFA, Sigma, St Louis, MO) in PBS (pH 7.4) for 24 hours before transfer into 30% sucrose in PBS for 48 hours at 4°C. The coronal brain sections were collected using a cryostat (Leica) on positively charged slides (Fisher Superfrost Plus), 30 µm thick sections specifically focusing on the CA1 subregion of the hippocampus. Following the immunostaining of frozen sections with eGFP antibody, DAPI containing Fluoro-Gel mountant was used for preserving the brain sections for imaging. The images were scanned after 1 hour using a VS120 (Olympus) scanner to assess the injection and expression of the virus in the CA1 subregion in the brain sections. All images were captured at 20X magnification. Only animals with verified expression of the virus in the CA1 subregion of the hippocampus were included in the statistical analyses of behavioral data.

Statistics

The statistical analysis was performed using unpaired, two-tailed Student's t test to compare the two groups and one-way ANOVA followed by a post hoc Tukey test, Dunnett's test, Holm-Sidak test or Fisher's LSD test as stated. All analyses were performed using GraphPad Prism version 8 (details provided in the Supplemental tables). The results are presented as the mean \pm SEM throughout the text unless otherwise noted.

QUANTIFICATION AND STATISTICAL ANALYSIS

Statistical analyses of all data described in this study are available in Table S1. P values were calculated in GraphPad Prism and derived using unpaired two-tailed Students' t test or one-Way ANOVA. Tukey tests were used for post hoc analyses. Significance was defined as p < 0.05. The numbers of replications 'n" and statistical tests used are described in each Figure.